

A VIBRATIONAL STUDY OF A SELECTED SERIES
OF MATRIX-ISOLATED ALKALI-METAL
CHLORATE AND NITRATE SALTS

By

NORMAN RAY SMYRL
"

Bachelor of Science
West Texas State University
Canyon, Texas
1969

Master of Science
West Texas State University
Canyon, Texas
1971

Submitted to the Faculty of the Graduate College
of the Oklahoma State University
in partial fulfillment of the requirements
for the Degree of
DOCTOR OF PHILOSOPHY
December, 1973

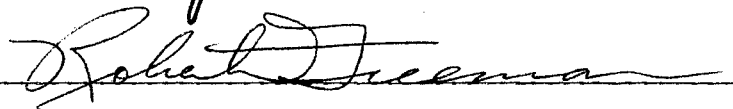
Thesis
1973D
S66TV
cop: 2

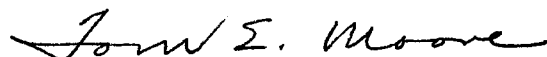
MAR 14 1975

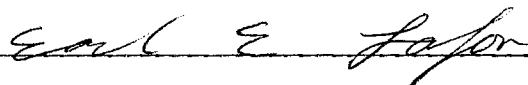
A VIBRATIONAL STUDY OF A SELECTED SERIES
OF MATRIX-ISOLATED ALKALI-METAL
CHLORATE AND NITRATE SALTS

Thesis Approved:


Thesis Adviser









Dean of the Graduate College

902238

ACKNOWLEDGEMENTS

Grateful acknowledgement is made to Dr. J. Paul Devlin, thesis director, for continuing assistance and guidance throughout this work.

I would like to express my love and gratitude to my wife, Sherry, for her encouragement and understanding throughout my tenure in graduate school and for her patient assistance in the preparation of this manuscript.

I would also like to gratefully acknowledge the financial support during this work provided by the National Science Foundation and Oklahoma State University.

Finally, I would like to thank Wayne Adkins and Heinz Hall for their aid in the design and repair of equipment utilized for this study.

TABLE OF CONTENTS

Chapter	Page
I. INTRODUCTION	1
Scope of the Problem.	1
Matrix Isolation.	3
Infrared Matrix Isolation.	3
Raman Matrix Isolation	5
Chlorates	6
The Symmetry and Selection Rules for the Chlorate Anion	7
Alkali-Metal Chlorate Aqueous Solutions and Melts.	8
Normal Coordinate Calculations	11
Glass Transition Temperatures	13
II. EXPERIMENTAL	17
The Cryostat.	17
Procedure	23
Instrumentation	27
III. EXPERIMENTAL RESULTS AND DISCUSSION	28
Matrix-Isolated Alkali-Metal Chlorates.	28
Potassium Chlorate	28
Sodium Chlorate.	38
Lithium Chlorate	47
Discussion	57
Matrix-Isolated Lithium Nitrate	61
Alkali-Metal Nitrate Glass Transition Temperatures.	65
IV. NORMAL COORDINATE CALCULATIONS	69
MClO ₃ Monomers.	69
The Model and the Force Field.	70
The Calculations	72
Discussion	79
LiNO ₃ Monomer	80

TABLE OF CONTENTS (Continued)

Chapter	Page
V. SUMMARY AND CONCLUSIONS.	88
Matrix-Isolated Alkali-Metal Chlorates.	88
Alkali-Metal Nitrates	89
Volatilization of Polyatomic Salts.	90
Correlation with Melt Spectra	91
SELECTED BIBLIOGRAPHY	93

LIST OF TABLES

Table	Page
I. Fundamental Frequency Assignment for the Unperturbed Chlorate Anion.	8
II. ν_3 Splittings and Force Constant Variations for the Alkali-Metal Nitrate Monomers	13
III. Deposition Temperatures for the Alkali-Metal Chlorate and Nitrate Salts	24
IV. Observed Frequencies (cm^{-1}) for Matrix-Isolated Vapors of Potassium Chlorate	35
V. Observed Frequencies (cm^{-1}) for Matrix-Isolated Vapors of Sodium Chlorate.	43
VI. Observed Frequencies (cm^{-1}) for Matrix-Isolated Vapors of Lithium Chlorate	55
VII. Observed Frequencies (cm^{-1}) for the Alkali-Metal Chlorate Monomers Isolated in Both Argon and Xenon	60
VIII. The Observed Infrared Frequencies for the Lithium Nitrate Monomer Matrix Isolated in Argon.	64
IX. Nitrate Glass Transition Temperatures	67
X. Calculated Frequencies and Potential Energy Distribution for the Lithium Chlorate Monomer.	75
XI. Force Constants Used for the Alkali-Metal Chlorate Monomers.	76
XII. Calculated Frequencies and Potential Energy Distribution for the Sodium Chlorate Monomer	77
XIII. Calculated Frequencies and Potential Energy Distribution for the Potassium Chlorate Monomer.	78
XIV. Observed ν_3 Splittings in Argon and Force Constant Variations for the Alkali-Metal Chlorate Monomers	80
XV. Calculated Frequencies and Potential Energy Distribution for the Planar Modes of the Lithium Nitrate Monomer	84

LIST OF TABLES (Continued)

Table	Page
XVI. Calculated Frequencies and Potential Energy Distribution for the Planar Modes of the Lithium Nitrate Monomer . . .	85
XVII. Force Constants Used for the Alkali-Metal Nitrate Monomer .	86

LIST OF FIGURES

Figure	Page
1. The Cryostat Cooling and Sampling Assembly	19
2. The Cryostat Vacuum Hardware	21
3. Oven Assembly.	22
4. Raman Illumination Geometry.	26
5. Infrared Bands for ν_1 and ν_3 Modes of KClO_3	29
6. The Infrared Spectra of KClO_3 in Ar at 12°K with Different M/A Ratios	32
7. The Infrared Spectrum of KClO_3 Matrix Isolated in Xe at 12°K .	34
8. Raman Bands for ν_1 and ν_3 Modes of KClO_3 Isolated in Ar and Xe	36
9. Infrared Spectrum of NaClO_3 Matrix Isolated in Ar.	39
10. Infrared Spectrum of NaClO_3 Matrix Isolated in Xe.	41
11. Raman Bands for ν_1 and ν_3 Modes of NaClO_3 Matrix Isolated in Ar at 12°K	45
12. Infrared Spectrum of LiClO_3 Matrix Isolated in Ar.	48
13. The Infrared Spectrum of LiClO_3 Matrix Isolated in Xe at 12°K	50
14. Infrared Spectrum of ClO_2 Matrix Isolated in Ar at 12°K Generated by an Attempt to Vaporize AgClO_3	51
15. The $890\text{-}1000\text{-cm}^{-1}$ Region of the Raman Spectrum for the LiClO_3 Vapors Matrix-Isolated in Ar at 12°K	53
16. The Infrared Spectrum of LiNO_3 Matrix Isolated in Ar	63
17. Infrared ν_2 Band of LiNO_3 at the Glass-Crystallization Temperature.	66
18. Geometry and Internal Coordinates for the MClO_3 Monomer.	71
19. Geometry and Planar Internal Coordinates for the LiNO_3 Monomer	82

CHAPTER I

INTRODUCTION

Scope of the Problem

Vibrational spectroscopy has been used extensively to investigate the structure of aqueous electrolyte solutions and molten electrolytes. Much of the work has been concentrated on molten and aqueous nitrate systems (1) (2). Recently, however, some limited investigations involving chlorate systems have been reported (3) (4) (5) (6) (7). The vibrational spectra of both the nitrate and chlorate anions are particularly sensitive to various environments; thus, each of these anions is quite valuable as a structural probe. Various structural models have been suggested for the dilute and concentrated aqueous solutions and molten salts, but only the models for the dilute solutions seem to be well established. Most of the models are based to some extent on environmental perturbation of the anion in order to explain certain of the observed spectral features.

In determining the role that anion distortion plays in the spectra for various environments, it is of interest to consider the maximum possible distortion for a given case. For the alkali-metal nitrates or chlorates, the maximum distortion should occur when the anion is associated independently with only one cation. The vibrational spectra of such monomeric species have been observed for the matrix-isolated vapors of the alkali-metal nitrates (8) and indeed indicate a maximal distortion

of the nitrate anion. From this limiting case it is possible to make correlations with the nitrate melt and aqueous solution systems. This type of study has not been extended to the chlorates, and it would seem that such an investigation is warranted. The major phase of the present work will, therefore, be directed toward obtaining the vibrational spectra of a series of monomeric alkali-metal chlorates by the matrix-isolation technique. Although infrared spectroscopy is the method which has been used almost exclusively for the vibrational study of matrix-isolated species and will be the primary method used for the present investigation, attempts will be made to obtain Raman spectra of these species. Some pertinent normal coordinate calculations will also be included in this study.

In a later paper on the alkali-metal nitrates (9), it was reported that reduction of the matrix gas to nitrate ratio well below the value required for complete monomeric isolation results in the formation of aggregates of the isolated species. Comparison of the vibrational spectra of these aggregates with published melt spectra indicated a glassy rather than crystalline structure. It was further discovered that deposition of the metal nitrate vapors at liquid nitrogen temperature, in the absence of matrix gas, results in the formation of pure glass thin films. The preparation of thin film glasses by vapor deposition onto a cold substrate affords the rare opportunity for determination of glass transition temperatures for the pure alkali-metal nitrate glasses, which up to this date have only been determined "experimentally" from extrapolation of binary solution (hydrate melt) data (10). The second phase of the present investigation will, therefore, be concerned with the preparation of the alkali-metal nitrate thin film glasses and subsequent

determination of the glass transition temperatures by spectroscopic observation of the glass crystallization phenomenon. Attempts will be made to extend these determinations to the alkali-metal chlorates as well, if such thin film glasses can be prepared for these salts.

Matrix Isolation

Infrared Matrix Isolation

The matrix-isolation technique was originally proposed by Whittle, Dows, and Pimentel (11) for the study of unstable species, primarily free radicals, by infrared spectroscopy. Since that time, the method has been applied not only to a wide range of unstable molecules, radicals, and ions, but to stable molecules as well. The matrix-isolation technique involves the simultaneous condensation of an inert matrix gas (M) and a molecular beam of the species of interest (A), and the temperature must be low enough to provide a rigid matrix so that the molecules of A cannot associate by diffusion.

Of prime importance in the matrix-isolation experiment is the choice of a suitable matrix material. The material should, of course, be non-reactive with the isolated species and reasonably transparent in the infrared region to prevent complications in the spectra due to matrix absorptions. The matrix material should also have a low sublimation energy and a relatively high thermal conductivity so that heat produced by the condensation at the cryotip can be dissipated rapidly. The matrix materials most often utilized are the noble gases (Ne, Ar, Kr, Xe) and nitrogen. Very low substrate temperatures are required for these materials and are normally obtained through the use of liquid helium (4°K) or liquid hydrogen (20°K). Recently miniature Joule-Thompson refrigerators,

which are capable of providing the necessary low temperatures, have become available commercially and are being utilized to some extent in matrix-isolation experiments.

The infrared matrix spectra are normally characterized by very sharp fundamental features often accompanied by well resolved isotopic structure. The rotational structure normally appearing in vapor spectra is not observed, with the exception of some very small molecules which can still rotate in the matrix cage. Although valuable moment of inertia data is lost, the matrix spectra are much simpler and more easily analyzed. The matrix spectra may often be complicated by multiple frequencies due to multiple trapping sites. This effect is normally not serious and can be easily recognized by varying the matrix material. Frequencies in the matrix spectra may be shifted from vapor state values due to interaction of the isolated species with the matrix. These shifts are often negligible for nonpolar species but can be quite significant for polar molecules.

The infrared matrix-isolation technique and its numerous applications have been extensively reviewed by various authors recently (12) (13) (14) (15). This particular topic, thus, need not be developed any further except for a brief discussion of the application to high-temperature inorganic species which is, of course, pertinent to the present problem.

The matrix technique was first successfully adapted to inorganic molecules vaporizing at high temperatures by Linevsky (16). For this particular application, the molecular beam of the species to be isolated originates from a heated Knudsen cell. The experimental difficulties in measuring the infrared spectra of vapors at very high temperatures can

be avoided by this technique. Complications in the high-temperature vapor spectra due to highly excited vibrational-rotational structure is also avoided. The method is particularly well suited for study of species with very low vapor pressures.

Raman Matrix Isolation

In general, both the infrared and Raman spectra are required for absolute structural proofs and vibrational assignments; thus, the Raman spectra of matrix-isolated species would in many cases be of great value. However, until recent advancements in the technology of Raman spectroscopy, its use as a method for the study of matrix-isolated species was out of the question. Even with the development of high power laser sources and very sensitive detection systems, the task of obtaining good matrix Raman spectra remains a formidable one.

Some success has been reported recently by several groups that have been working on the Raman matrix-isolation problem. The general technique and some of the more troublesome problems associated with it have been discussed in several of these reports (17) (18) (19). The Raman matrix technique, as it now stands, consists of depositing the matrix film onto a highly polished metal surface and then using the single reflection technique described by Levin (20) to excite the matrix sample. Since Raman scattering is inherently a weak effect and the emissions from a dilute sample are even weaker, pains must be taken to maximize the Raman scattering and at the same time minimize the background signal.

The best results in regard to maximizing the Raman signal seem to be achieved for the more transparent matrix samples. The angle of incidence of the laser beam has also been shown to be an important factor

with maximum signals occurring for angles of incidence of 10 to 30° (18). The two main sources of high background signal are fluorescence and primary reflective scattering. Fluorescence is normally due to vacuum grease or other impurities, so careful pains must be taken to avoid such contaminants. Primary scattering can be effectively reduced through the use of the appropriate optical filters.

Although the film thickness required for Raman studies is two to three times that required for normal infrared matrix work, laser heating has not been shown to be a problem at least for the transparent nonabsorbing matrix film. The measurement of depolarization ratios, which are particularly valuable in making band assignments, is possible for matrix samples (18) (19). These measurements are normally enhanced for the more transparent films.

Included among the systems which have been studied thus far by the Raman matrix-isolation technique are such high-temperature species as MX_2 and MXY (where $\text{M} = \text{Ge, Pb, Sn}$ and $\text{X, Y} = \text{Cl, Br}$) (19), SeO_2 (21), PrF_3 (22), and MNO_3 (where $\text{M} = \text{alkali metals}$) (8) (9). Other systems which have been studied include the molecules XeCl_2 (23), XeO_3F_2 (24), BeB_2H_8 (25), and LiO_2 (26) and the radicals Br_3 (27) and OF (28). Although the single reflection technique has yielded significant results, the ultimate answer to the Raman matrix isolation problem may lie in some type of multireflection or beam trapping technique. Some work is currently under way in this particular area (29).

The Symmetry and Selection Rules
for the Chlorate Anion

It has been well established by Raman, infrared, and x-ray methods that the chlorate anion has a symmetrical pyramidal structure, thus, the unperturbed anion belongs to the C_{3v} symmetry point group. There are six possible vibrational modes for the tetratomic chlorate anion, and these are classified as $2A_1 + 2E$ by symmetry selection rules, the E modes being doubly degenerate. The four fundamental frequencies are both infrared and Raman active with the A_1 and E modes being Raman polarized and depolarized, respectively. Any deviations from these selection rules, particularly splitting of degenerate modes, can be interpreted as resulting from the lowering of the point group symmetry by destruction of the C_3 rotation axis. The C_{3v} symmetry selection rules for the chlorate anion are essentially obeyed at low resolution in the dilute aqueous solution spectrum with fundamental frequencies corresponding to those appearing in Table I.

As previously mentioned the alkali-metal chlorates are to be the focus of the major phase of the present work. It should be possible, in a manner similar to the alkali-metal nitrates (8), to vaporize the chlorate salts (Li,Na,K) at temperatures just above their respective melting points and subsequently matrix isolate the vapor species, of which the monomeric form should be a major constituent. In the monomeric form there will be no intermolecular interaction; thus, the vibrational spectrum should be free of any complications due to such interactions. Providing the cation coordinates through an oxygen atom, the chlorate ion should undergo a maximum distortion due to the association with a

single cation. In this case the C_{3v} symmetry of the chlorate anion would be lowered most probably to C_s , and the vibrational spectrum should show significant changes, i.e., frequency shifts and in particular splitting of the degenerate ν_3 and ν_4 modes. It should be possible to relate the extent of the splitting to the magnitude of the distortion and, in turn, to the strength of the forces causing the distortion. Such results should help to determine to what extent the interactions in the melts and aqueous solutions involve distortion of the anion.

TABLE I
FUNDAMENTAL FREQUENCY ASSIGNMENT FOR THE
UNPERTURBED CHLORATE ANION

Mode	Assignment	Frequency ^a (cm^{-1})
$\nu_1(A_1)$	symmetric stretch	930
$\nu_2(A_1)$	symmetric deformation	610
$\nu_3(E)$	asymmetric stretch	982
$\nu_4(E)$	asymmetric deformation	479

^aThe Frequencies are Raman Dilute Solution Values from Reference (30).

Alkali-Metal Chlorate Aqueous Solutions
and Melts

The vibrational studies involving the alkali-metal chlorate melts and aqueous solutions have been very limited, particularly with respect

to the large amount of work that has been done on the alkali-metal nitrate systems (1) (2). The chlorate melts have been examined by both infrared and Raman spectroscopy; however, as with the nitrate systems, the interactions prevalent in these melts are not clearly understood. In the infrared reflection work of Wilmhurst (3), LiClO_3 exhibited the only detectable splitting of degenerate modes, with a split of approximately 41 cm^{-1} for ν_3 being observed. Since no splitting was observed for either NaClO_3 or KClO_3 , associated species of type M-O-ClO_2 were ruled out. It was suggested rather that the splitting observed for LiClO_3 was due to removal of the C_3 axis by the asymmetric cation field and inhibition of free rotation about this axis. The observation of a low frequency lattice-like band at 338 cm^{-1} for LiClO_3 led Wilmhurst to suggest a quasi lattice-like structure. The existence of such bands for NaClO_3 and KClO_3 was postulated, but an instrumental cut-off at 220 cm^{-1} may have prevented their observation. It should be pointed out that such a lattice-like structure as was suggested does not imply any long range ordering like in the crystal.

Similar conclusions to those of Wilmhurst were later reached in the Raman work of James and Leong (4). Only the Raman spectrum of LiClO_3 melt exhibited any splitting of degenerate modes with ν_4 being split but not resolved. The ν_3 mode was also presumably split although not observed due to the overlap of this mode by the very intense ν_1 band. It was further noted by these authors that the Raman and infrared frequencies for the alkali-metal chlorate melts are possibly non-coincident, thus implying that the vibrating unit possesses a center of symmetry.

With improved instrumentation over those authors of reference (3) and (4), Bates, et al. (7), in their Raman and infrared emission work on

NaClO_3 and KClO_3 , showed that these melts also exhibit the splitting of the degenerate ν_3 and ν_4 modes. Weak bands were also observed between ca. 80 and 200 cm^{-1} in the Raman spectra of both molten NaClO_3 and KClO_3 and assigned to anion libration. A similar band at 140 cm^{-1} has also recently been observed in the Raman spectrum of LiClO_3 melt by Oliver and Janz (5). The combined spectral data for the chlorate melts seem to indicate that the same type perturbations observed for the NO_3^- ion in the alkali-metal nitrate melts are also observed for the ClO_3^- ion in the alkali-metal chlorate melts. The origin of certain of these spectral effects is still the subject of much controversy among various groups involved in molten salt spectroscopy.

The aqueous electrolyte solutions potentially have the greatest chemical significance; thus, an understanding of the interactions prevalent in such solutions is very important. There is an acute shortage of vibrational data for the aqueous alkali-metal chlorate solutions. Even so, the interactions in the dilute solutions appear to be well understood. A solvent-anion interaction probably of an H-bonding nature appears to be present even at high dilutions causing a significant splitting of ν_3 (5) (6). For LiClO_3 , Oliver and Janz (5) observed a constant splitting of approximately 34 cm^{-1} for ν_3 as the concentration range was varied from very dilute up to 5M. Apparently the distortion is not great enough for ν_4 to be observably split.

As has been shown for the alkali-metal nitrates (2), the interactions in the more concentrated solutions are more difficult to interpret. It should be noted at this point that vibrational spectra of the ultra-concentrated solutions often mimic the pure melt spectra. The only greatly significant data to be reported in the literature for the

more concentrated alkali-metal chlorate solutions is that work of Oliver and Janz (5) on LiClO_3 and that of Bates, et al. (7), on NaClO_3 and KClO_3 . Using a resolution of band contours technique, Oliver and Janz observed an increasing split of ν_3 from 34 cm^{-1} to 55 cm^{-1} in the Raman aqueous solution spectra of LiClO_3 as the concentration range was increased from 5M to 17.1M. Over the same concentration range a constant split of ca. 20 cm^{-1} was observed for ν_4 with the higher frequency component continually gaining intensity until it almost equals that of the lower component at 17.1M. Also the low frequency band at 140 cm^{-1} in the melt spectrum is no longer observed. No definite conclusions were reached regarding the interactions prevalent in the more concentrated solutions of LiClO_3 ; however, the authors do state that for the more concentrated solutions a competition probably exists between water molecules and ClO_3^- ions for sites in the inner coordination sphere of the Li^+ ions due to an insufficiency of water. Bates, et al. (7), have obtained the Raman and infrared absorption spectra of saturated solutions of NaClO_3 and KClO_3 and the ν_3 and ν_4 modes of ClO_3^- were observably split.

It is readily apparent that much more work needs to be done before the concentrated solutions and melts are clearly understood. The present work involving the matrix-isolated alkali-metal chlorates hopefully will be of some use in clarifying this situation.

Normal Coordinate Calculations

As mentioned previously, normal coordinate calculations will be made on a model representing the alkali-metal chlorate monomer. Rather than merely obtaining a fit of the observed frequencies, it is hoped

that such calculations will yield reasonable estimates of changes in the force field relative to the unperturbed (C_{3v}) anion necessary to fit the observed spectral splittings for the degenerate modes. Calculations of this type have been performed on the matrix-isolated alkali-metal nitrate monomers (8). Since there are obvious parallels that can be drawn between the nitrate and chlorate cases, it would appear that a brief review of the results obtained for the alkali-metal nitrate monomers is in order at this point.

The unperturbed nitrate anion has a trigonal planar structure and belongs to the D_{3h} symmetry point group. The nitrate anion, like the chlorate anion, is tetratomic and, thus, has six possible vibrational modes classified as $A_1' + A_2'' + 2E'$. As is the case for the chlorate anion the ν_3 and ν_4 modes of the nitrate anion belong to the doubly degenerate E symmetry species. These modes retain their degeneracy as long as the C_3 rotation axis remains intact. In the case of the matrix-isolated alkali-metal nitrate monomer, the association of the nitrate anion with a single cation effectively destroys the C_3 axis, thus removing the degeneracy of the ν_3 and ν_4 modes. The magnitudes of the ν_3 splittings which are observed in the infrared spectra of the alkali-metal nitrate monomers are given in Table II. Also given in Table II are the variations in the force constants K_1 and K_2 determined by normal coordinate calculations for the various alkali-metal nitrate monomers utilizing a Urey-Bradley type force field, where K_1 is the stretching constant for the two unassociated N-O bonds and K_2 is the stretching constant for the lone associated N-O bond. The quantity $(2K_1 + K_2)$ was constrained to a constant value in the calculations in order to maintain a fixed total amount of bonding. The difference in K_1 and K_2 , given in

the table by ΔK , can be seen to increase through the group from Rb to Li. It was shown that this trend qualitatively agrees with the trend established for the polarizing powers of the various alkali-metal cations. ΔK is, thus, presumed to represent a rough measure of the cation polarization of the anion. From these results, it is concluded that cation polarization is the dominant source of anion distortion for the alkali-metal nitrate monomers.

TABLE II
 ν_3 SPLITTINGS AND FORCE CONSTANT VARIATIONS FOR
 THE ALKALI-METAL NITRATE MONOMERS^a

M^+	$\Delta\nu_3$ (cm^{-1})	K_1 ($\text{mdyne}/\overset{\circ}{\text{A}}$)	K_2 ($\text{mdyne}/\overset{\circ}{\text{A}}$)	ΔK ($\text{mdyne}/\overset{\circ}{\text{A}}$)
Li	240	7.57	2.87	4.70
Na	201	7.12	3.77	3.35
K	171	6.87	4.27	2.60
Rb	163	6.82	4.37	2.45

^aResults from Reference (8).

Glass Transition Temperatures

The investigation of the glassy state is fast becoming an important general branch of the physicochemical science. This rapid growth is due primarily to the discovery and utilization of new types of glasses. It

is now realized, also, that the glassy state occurs quite generally in nature, and examples are known for every class of chemical substance.

At one time the glass-forming ability of a material was focused primarily on structural aspects, whereas now it is realized that the most fundamental aspect in determining the transformation of a substance from a liquid to the glassy state is a thermodynamic one. Even with the growth and new understanding of the glassy states, no rigid definition which comprehensively covers all glasses has yet been established. Probably the most acceptable definition of a glass is any solid-like material which is amorphous to x-rays and undergoes a pseudo-second order thermodynamic phenomenon known as the glass transition (31). At the glass transition the material undergoes a rather abrupt increase in its intensive thermodynamic properties from solid-like to liquid-like values. Also at the glass transition and temperatures below the glass transition, the viscosity of the material is very high, about 10^{13} poise (32). Based on the observation first made by Kauzmann (33), that in general a super cooling liquid tends to lose entropy at a more rapid rate than does the stable crystalline phase over the same temperature range, it is readily apparent that a process such as the glass transition must inevitably occur so that the liquid does not reach a lower state of entropy than the crystal before the temperature falls to 0°K .

The temperature at which the glass transition occurs is referred to as the glass transition temperature (T_g) and is the most directly measurable parameter associated with the transition. Since the process occurs under non-equilibrium conditions, T_g is not a true thermodynamic transition temperature. T_g is, however, of thermodynamic interest due to its close relationship to the theoretical or "ideal" glass transition

temperature (T_0), which is obtained by extrapolation of equilibrium thermodynamic data. Glass transition temperatures are also very useful in predicting and interpreting other physicochemical properties such as transport phenomena.

The definition of the glassy state as stated previously includes not only glasses obtained by super cooling of liquids but those obtained by other methods as well. As mentioned in an earlier section of this chapter, the second phase of the present investigation will involve the measurement of glass transition temperatures for the pure alkali-metal nitrate thin-film glasses obtained by vapor deposition. Although such measurements are not directly related to the matrix-isolation problem, there appears to be some justification for including such a study in the present work. First of all, the preparation of the pure alkali-metal nitrate glasses by the vapor deposition technique provides a rare opportunity for the measurement of glass transition temperatures, since prior attempts to prepare amounts of pure glasses necessary for T_g measurements have largely been unsuccessful. Secondly, little, if any, alteration in the experimental set-up used for the matrix-isolation problem is required.

Although glass transition temperatures are normally measured calorimetrically, the T_g measurements in the present study are to be determined by spectroscopically observing the glass-crystallization phenomenon. The use of the glass-crystallization temperature as a measurement of T_g for glasses obtained by methods other than supercooling of the liquid can be justified. Sugisaki, et al. (34), observed for vapor-deposited glassy methanol a glass transition at 103°K denoted by a sudden increase in heat capacity, followed very closely at 105°K by an

irreversible crystallization. The same authors observed a similar behavior for vapor-deposited glassy water (35) which exhibited a glass transition at 135°K followed by an irreversible crystallization at the same temperature. It has been noted by Angell (36) that crystallization temperatures, which appear to precede any manifestation of the glass transition, have also been observed by others working with glassy films obtained by splat quenching from liquids as well as deposition from the vapor. He also notes, however, that the difference should not be too great. It has been postulated that T_g is probably the lowest temperature at which significant rearrangement of molecules or ions in the condensed phase can occur (10). The glass-crystallization temperature, thus, should be a very close estimate of the glass transition temperature.

CHAPTER II

EXPERIMENTAL

The Cryostat

The experimental portion of this work consisted primarily of two phases. The first phase involved the preparation of a series of alkali-metal chlorate monomers using the high-temperature matrix-isolation technique and subsequent characterization of these species by infrared and Raman spectral measurements. Also included in the matrix work are some further studies involving LiNO_3 for comparison with the MClO_3 data. The second phase involved the preparation of the thin-film glasses of the alkali-metal nitrates and subsequent determination of the glass transition temperatures by spectral observation of the glass-crystallization process. Both experimental phases involved low-temperature deposition of vapor species, thus requiring a cryostat of suitable design.

As previously mentioned in the introductory chapter, miniature Joule-Thompson refrigerators capable of providing very low temperatures have recently become available commercially and are just beginning to be utilized in low-temperature spectroscopy. The cryostat utilized in the present investigation was designed around a Model CS-202 DisplexTM Helium Refrigerator manufactured by Air Products and Chemicals, Inc. The Displex unit is a closed-cycle cryogenic system employing commercial-grade helium as a refrigerant and is capable of providing various amounts of cooling from 12° to 300°K . The entire system consists of a two-stage

displacer/expander cryogenic cooler, an air-cooled, oil-lubricated compressor module, and an electrical control panel. The displacer/expander is connected to the compressor by means of flexible metal lines terminated with self-sealing couplings. The unit is charged with helium at a static pressure of ca. 220 psig. When the system is in operation, the compressor discharge pressure reaches ca. 320 psig. A special charging manifold is provided with the system for refilling with helium should it become necessary.

A diagram of the Model CS-202 DisplexTM displacer/expander cooler and the attached spectroscopic sampling assembly appears in Figure 1. The displacer/expander weighs 16 lbs and can be mounted at any orientation. It has a net refrigeration at 70° to 80°F ambient temperature ranging from 5 watts at 77°K to 1 watt at 17°K. A variable internal heater at the cryotip permits any temperature in the range from 12° to 300°K to be accurately established. The cool-down time from 300° to 12°K requires 45 minutes under an insulation vacuum which must be maintained at less than 10^{-4} torr. The system is so designed that once maximum cool-down and the necessary deposition have been achieved, it can be removed from the vacuum line for the necessary spectroscopic studies. The compressor unit, which weighs 150 lbs, along with the electrical control panel are mounted on a movable cart for mobility purposes. The single most attractive feature of the entire system is probably its simplicity and ease of operation. The operation details and instructions and other pertinent information are provided in the technical manual which comes with the system (37).

The sampling assembly as shown in Figure 1 consists of a copper block which is attached to the cryotip. The CsI window needed for the

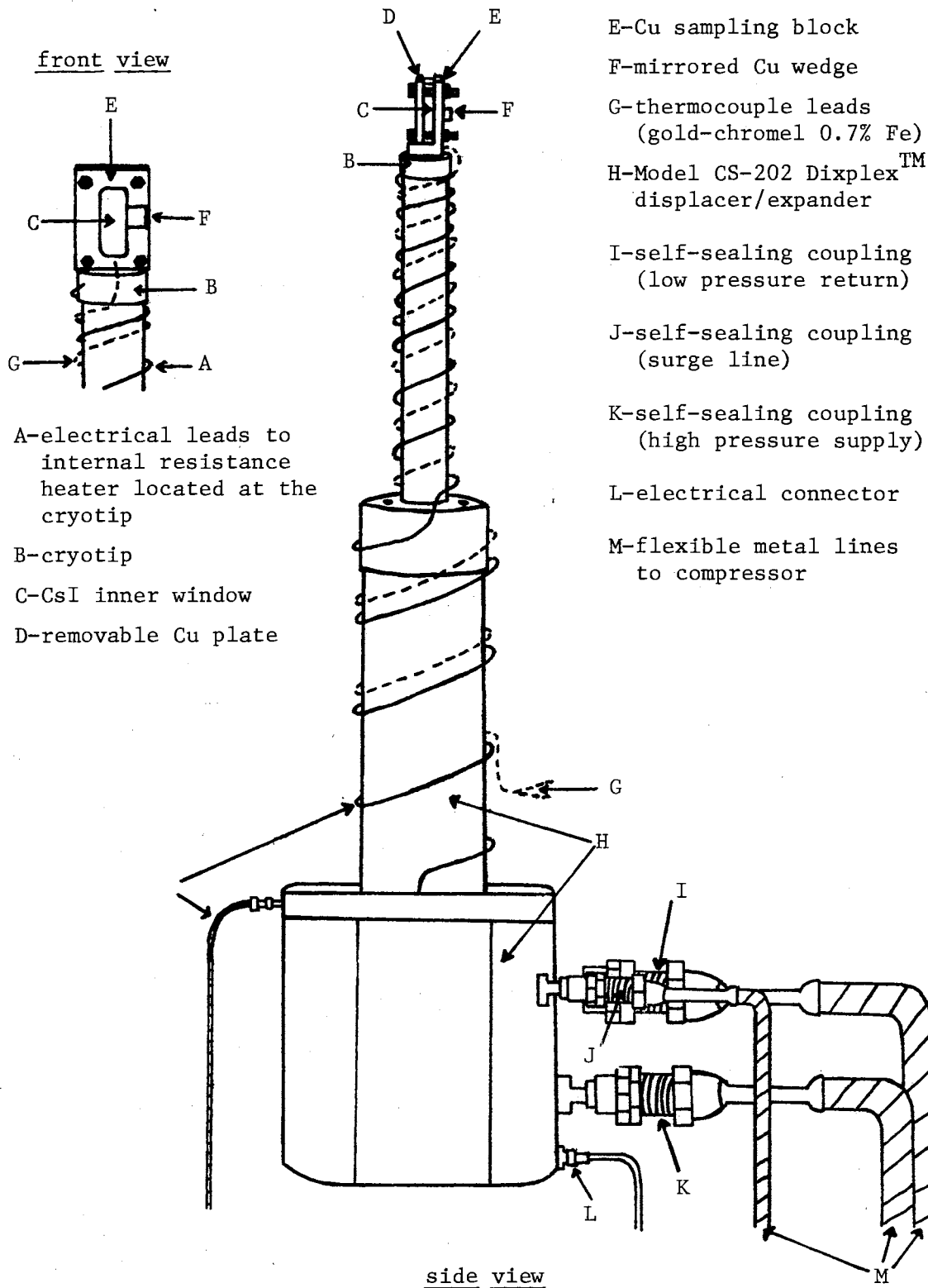


Figure 1. The Cryostat Cooling and Sampling Assembly

infrared transmission studies is held between the copper block and a removable copper plate by means of four screws. Thermal contact between the tip and the block, and the block and the window is maintained by thin indium gaskets. A small copper wedge inclined at an angle of ca. 10° is also attached to the copper block by means of a small screw for the single reflection Raman studies. The leads for a gold-chromel (0.7% Fe) thermocouple are imbedded in the copper block and packed with indium for temperature monitoring.

The cryostat vacuum hardware which was designed for the present studies is displayed in Figure 2. A brass shroud, which can be rotated by means of a bearing assembly, is mounted on top of a stainless steel shroud to which the displacer/expander is attached. The rotation of the upper shroud provides the necessary orientational capabilities for not only the sample deposition but also the infrared and laser Raman studies. All seals in the vacuum assemblage including the outer optical windows and the stainless steel oven port are made with O-rings. The windows, two of which are fashioned from CsI and the third from Pyrex, are held in place by threaded brass plates. The matrix-gas inlet consists of a small-diameter brass tube inserted through the wall of the upper shroud just below the oven port. A Kovar-to-glass seal connects this tube to the matrix-gas reservoir.

A detailed diagram of the oven assembly from which the salts are vaporized appears in Figure 3. The Knudsen oven consists of a Pyrex tube fitted with a 7/25 taper joint and is supported inside the bore of a 29/42 standard taper O-ring joint by a stainless steel plug in which a solid Pyrex rod fused to the male section of the 7/25 joint is inserted. The cell is heated by a coil of No. 24 chromel wire having a resistance

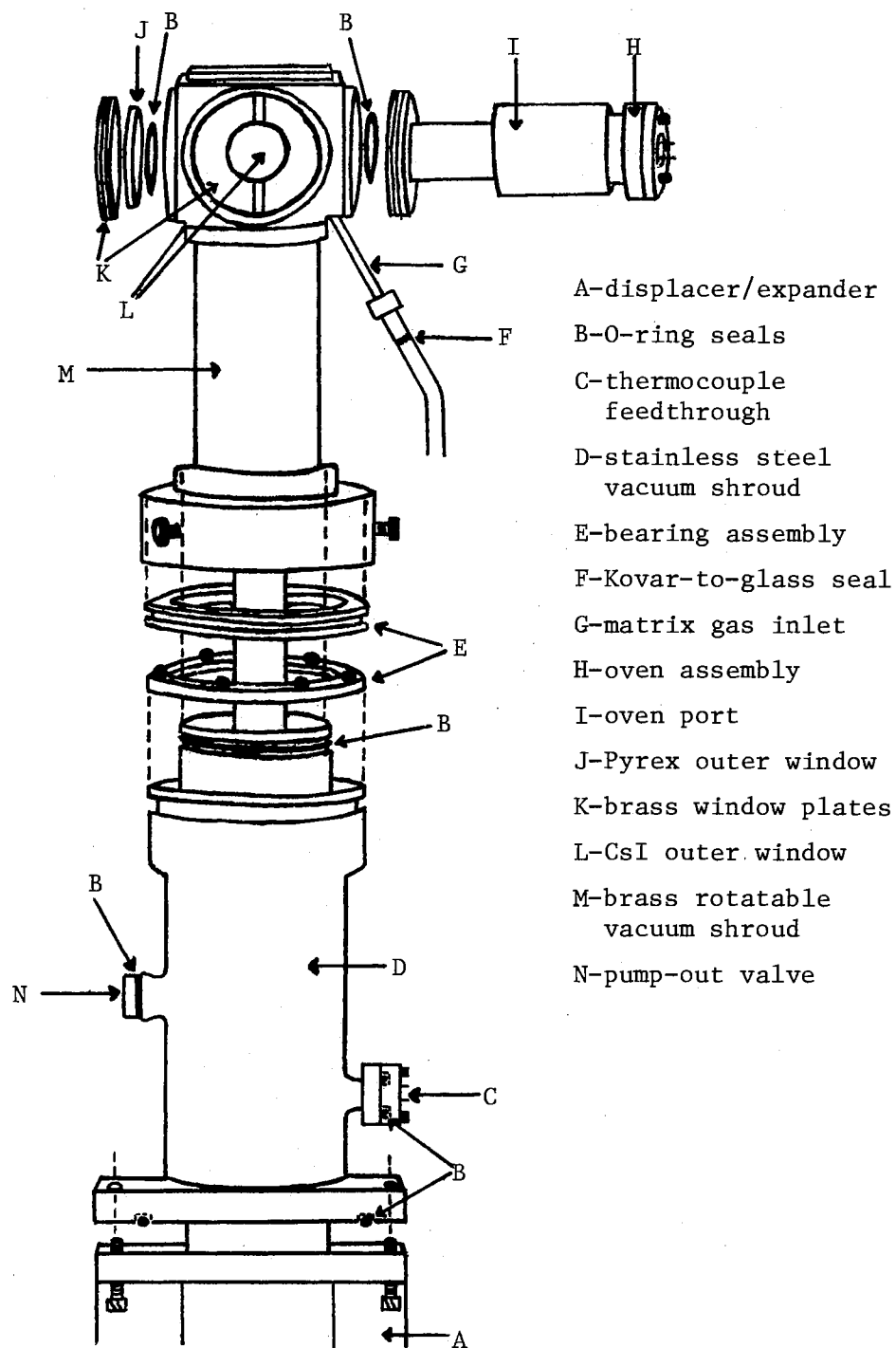
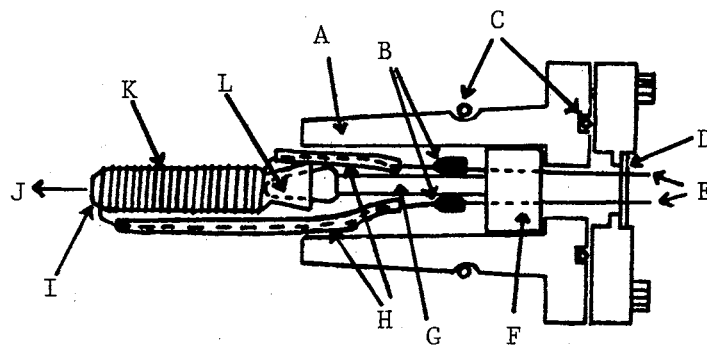


Figure 2. The Cryostat Vacuum Hardware



- | | |
|--|--------------------------------------|
| A-29/42 standard taper
O-ring joint | G-Pyrex rod |
| B-electrical contact clips | H-woven glass insulation |
| C-O-ring seals | I-Pyrex oven |
| D-ceramic feedthrough | J-vapor beam direction |
| E-Cu leads | K-chromel resistance heater |
| F-stainless steel support | L-7/25 standard Pyrex taper
joint |

Figure 3. Oven Assembly

of 9.5 ohms. The diameter of the effusion hole in the Pyrex oven is maintained at about 3 to 4 mm. The entire oven assembly inserts into the oven port which consists of a matching 29/49 standard taper joint.

Procedure

The typical matrix isolation experiment consisted of the simultaneous condensation of a molecular beam of the appropriate salt produced from the resistively-heated Pyrex Knudsen cell along with Ar or Xe onto the CsI inner window and the mirrored Cu wedge which were cooled to ca. 12°K. The salt was generally dried overnight at ca. 200°C under vacuum prior to deposition. The deposition times ranged from two to six hours, depending upon the thickness of the sample desired. Since precise control of the salt beam densities was not possible, the optimum M/A ratios were established by trial and error. As a general practice in the experimental procedure, the matrix gas was allowed to flow for a few minutes both prior to and after the deposition of the salts to insure good isolation. A slight variation in the above procedure consisted of omitting the deposition of the matrix gas which permitted the formation of the pure glassy films of the salts. The vacuum pressure was maintained at between 10^{-5} and 10^{-6} torr throughout the deposition process. Once deposition was complete, the cryostat was removed from the vacuum line so that the appropriate infrared and Raman spectral studies could be made.

A list of the salts which were studied at some juncture in the present investigation are presented in Table III along with the approximate deposition temperatures. All of the salts were commercial reagent grade salts which were used without further purification. Also given in Table III for reference are the melting points for the respective salts, and

one can easily see that the vaporization of all salts were made from the molten state.

TABLE III
DEPOSITION TEMPERATURES FOR THE ALKALI-METAL
CHLORATE AND NITRATE SALTS

Salt	Dep. Temp. ($^{\circ}\text{C}$)	Melt. Pt. ($^{\circ}\text{C}$)
LiClO_3	355	128
NaClO_3	355	248
KClO_3	410	356
AgClO_3	310	230
LiNO_3	410	264
NaNO_3	475	307
KNO_3	500	334
TlNO_3	255	206

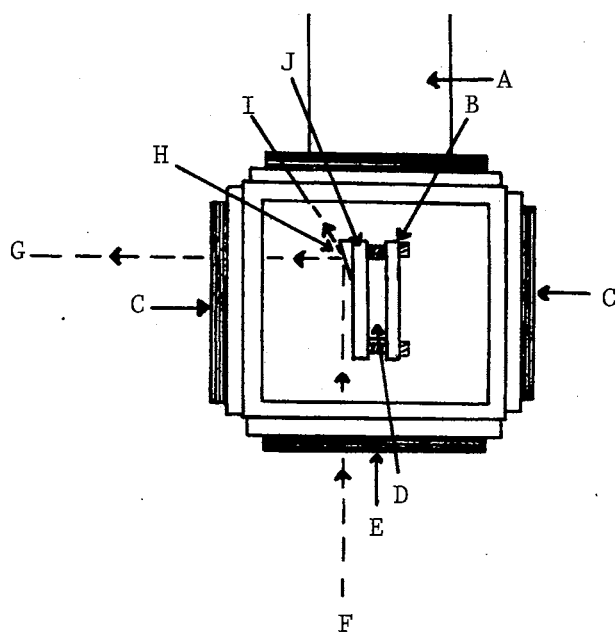
Due to the design of the Pyrex Knudsen oven, there was no place to attach a thermocouple for direct measurement of temperature during deposition of the salt. Deposition temperatures were, thus, established indirectly from the settings of two variacs arranged in series which served as the voltage supply for the oven heater. The primary variac was permanently set at 15 while the second variac was variable with a full-scale output of ca. 18.5 volts. A blank experimental run was made with

an iron-constantan thermocouple inserted through the effusion hole of the Pyrex Knudsen oven and packed snugly with glass wool. The temperature was observed to vary smoothly with changes in setting of the second variac. Settings of 20, 50, 80, and 120 were found to correspond to temperatures of 80° , 247° , 377° , and 508°C , respectively.

The matrix gases consisted of commercial grade Ar and research grade Xe which were used without further purification. During deposition the flow of these gases was controlled by a Fischer-Porter 1/16 glass flowmeter fitted with a sapphire float. For the preparation of samples with moderate thickness, the float was maintained at an average reading of about 4, which for Ar corresponds to a flow rate of ca. 0.2 millimoles/min.

The infrared spectra of the various matrix and glass samples were obtained by standard transmission methods. Raman scattering was obtained by the single reflection technique of Levin (20). The illumination geometry which was utilized for the Raman studies is illustrated in Figure 4. The incident laser beam was brought in through the Pyrex window and focused on the sample deposited on the mirrored Cu wedge. The scattered radiation was collected at ca. 90° from the incident beam through one of the CsI outer windows by an Auto Mamiya Sekor F 1.8 camera lens and focused onto the entrance slit of the monochromator.

As mentioned in the introductory chapter, high background signals are often a problem that must be confronted when making Raman measurements on highly dilute matrix films. Such a problem was encountered in the present study of the matrix-isolated alkali-metal chlorates. It was determined that the excessive background signals which were observed originated primarily from fluorescent sources. Reflective scattering was



- | | |
|------------------------|---------------------------|
| A - oven port | F - incident laser light |
| B - removable Cu plate | G - scattered light |
| C - CsI outer window | H - mirrored Cu wedge |
| D - CsI inner window | I - reflected laser light |
| E - Pyrex outer window | J - Cu sampling block |

Figure 4. Raman Illumination Geometry

ruled out as a possible source after the introduction of an optical filtering device between the condensing lens and the monochromator slit failed to significantly reduce the background signals. This filtering device was a Model 7155 Oriel Filter Monochromator that is variable over a wavelength range of 400 to 700 nm. Since all vacuum seals were essentially greaseless, the fluorescence problem probably resulted from trace amounts of decomposition product from the vaporization of the salts.

Instrumentation

The infrared spectra were recorded with a Beckman IR-7 spectrophotometer which is a prism-grating instrument that covers the range from 600 to 4000 cm^{-1} . A CsI interchange was available which permitted the frequency range to be extended down to 200 cm^{-1} .

Raman scattering was recorded on a system constructed around a Jarrell-Ash 25-100 dual monochromator fitted with an ITT FW-130 PM photomultiplier tube and Hamner photon counting gear. The Raman spectra were excited with a Coherent Radiation Model 52 argon ion laser using both the 5145 \AA (green) and 4880 \AA (blue) lines.

CHAPTER III

EXPERIMENTAL RESULTS AND DISCUSSION

Matrix-Isolated Alkali-Metal Chlorates

The anhydrous molten salts of the alkali-metal chlorates (Li, Na, K) have been found to volatilize in vacuum from a Knudsen oven with minimal decomposition except in the case of LiClO_3 . The vapor species above these salts have been characterized by infrared and Raman spectroscopy utilizing the matrix-isolation technique. The matrix-isolation experiments were performed in both Ar and Xe in order to determine the effects of different matrices. The spectra indicate that the alkali-metal chlorate monomeric species is a major constituent of the vapors, thus making a detailed study of the monomer modes possible. The best overall results appear to have been obtained for KClO_3 and, therefore, will be discussed first in considerable detail.

Potassium Chlorate

The $850\text{-}1150\text{-cm}^{-1}$ region of the infrared spectrum of KClO_3 isolated in Ar at 12°K appears in curve (a) of Figure 5. For comparative purposes, the infrared spectrum over the same spectral region for a pure thin film of KClO_3 vapor deposited in the absence of any matrix gas at ca. 100°K appears in curve (d) of Figure 5. Both of these curves exhibit strong absorption in the $900\text{-}1050\text{-cm}^{-1}$ region which is attributable to the ν_1 and ν_3 chlorate fundamentals. Decomposition appears to occur

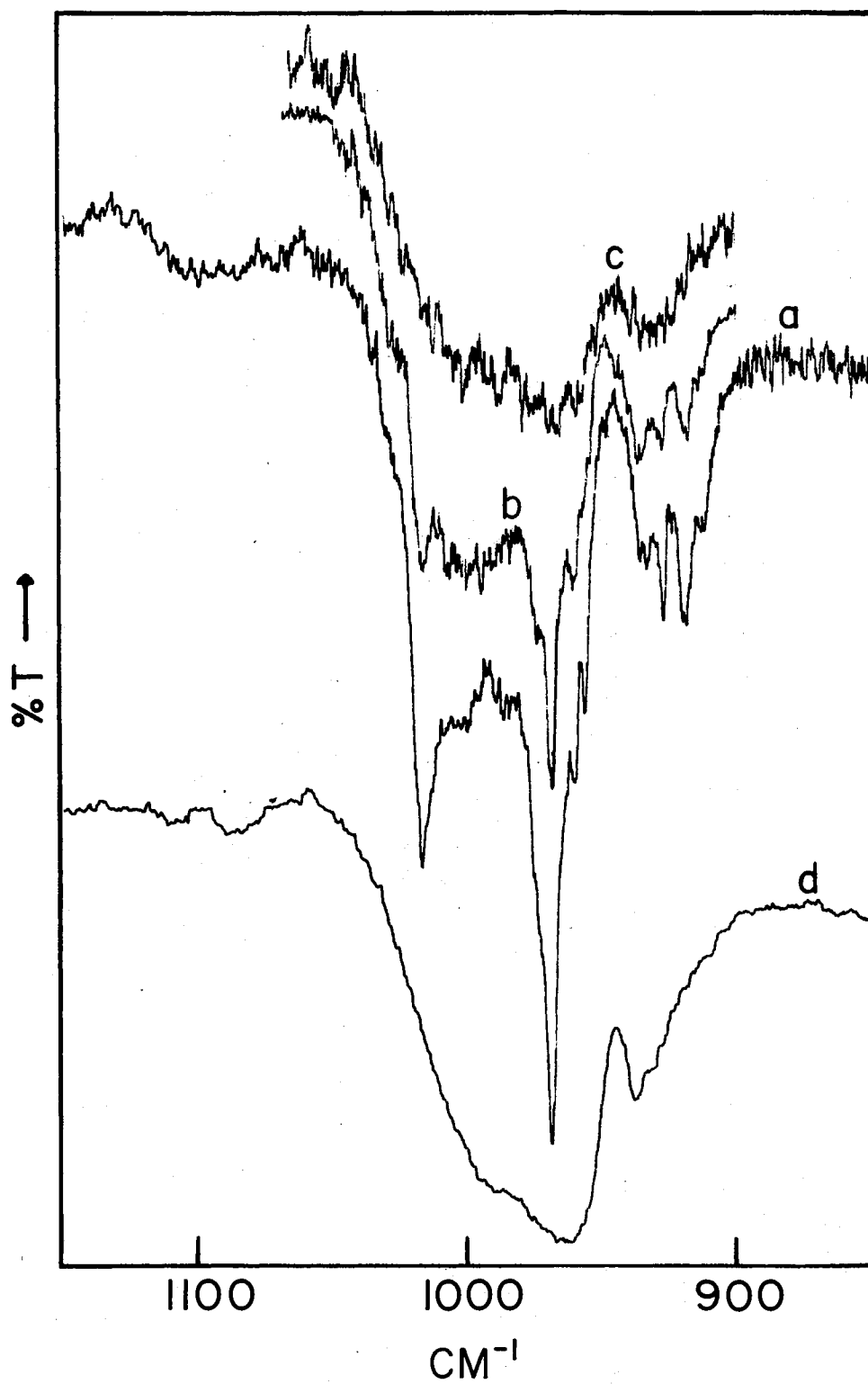


Figure 5. Infrared Bands for ν_1 and ν_3 Modes of KClO_3 : (a) matrix isolated in Ar at 12°K ; (b) matrix sample of curve (a) at 12°K after warming to ca. 35°K ; (c) matrix sample of curve (a) at 12°K after warming to ca. 50°K ; (d) pure film at ca. 100°K

only to a very minor extent on volatilization of KClO_3 as can be observed by the very weak feature near 1100 cm^{-1} in both curves (a) and (d). This feature as will be shown later in the discussion of LiClO_3 , is a good monitor of the amount of dissociation which occurs on volatilizing the alkali-metal chlorates.

The differences in curves (a) and (d) of Figure 5 are readily apparent with the matrix spectrum exhibiting some very sharp band structure as compared to the rather broad features of the pure thin film. Curve (a) shows very little further change on increasing the M/A ratio, thus indicating that maximum isolation has been obtained. Bands appearing in curve (a) at 917 , 927 , 968 , and 1017 cm^{-1} can be attributed to the KClO_3 monomeric species on the basis of the diffusion results given by curves (b) and (c) of Figure 5. These curves represent successive stages of warm-up in the matrix for the isolated sample of curve (a). The spectrum given by curve (b) was obtained after the sample had been warmed to ca. 35°K while that of curve (c) was obtained after the sample had been warmed to ca. 50°K . The set of bands previously mentioned appear to be diminished considerably in intensity in curve (b). The relative intensities of these bands do remain about the same as that observed in curve (a), thus indicating that these features belong to the same species. The 935-cm^{-1} band, which appears slightly weaker than the $917, 927\text{-cm}^{-1}$ doublet in curve (a), is quite obviously due to some polymeric species, most likely dimer, since its intensity appears to be somewhat enhanced relative to the monomer features in curve (b). A broad band which grows in at ca. 1000 cm^{-1} in curve (b) apparently can also be attributed to the same species. The observation of dimers in the vapors of the alkali-metal chlorates is not at all unexpected since

such species have been identified in both mass spectral (38) and matrix-isolation (8) studies of the alkali-metal nitrate vapors.

All of the sharp band structure appearing in curves (a) and (b) appears to have vanished in curve (c). The rather broad band structure which remains can be attributed to the formation of small KClO_3 aggregates in the matrix. It should be pointed out that curve (c) closely resembles the pure thin-film spectrum in curve (d). There is some indication that the structure of the low-temperature thin-film vapor deposit and the matrix aggregates is of a glassy nature much like that observed for the alkali-metal nitrates (9), although this has not been definitely confirmed in the present investigation.

By comparing curves (a) and (b) of Figure 6 which represent the infrared spectrum of KClO_3 in Ar at different M/A ratios, other monomer features can be identified. Curve (a) again represents a sample of near maximum isolation, while curve (b) represents a sample with an Ar to KClO_3 ratio well below that of curve (a). The dimer species previously identified is obviously present in much greater abundance relative to the monomer in the sample of curve (b) as evidenced by the 900-1050- cm^{-1} region of the spectrum. The 935- cm^{-1} dimer feature can be observed to dominate the 900-950- cm^{-1} region in curve (b), and, further, the 1017- cm^{-1} monomer feature has all but been absorbed in the broad dimer feature centered at ca. 1000 cm^{-1} . Shifting attention now to 450-650- cm^{-1} region where the ν_2 and ν_4 chlorate fundamentals are expected, bands at 495 and 611 cm^{-1} are observed to increase considerably in intensity relative to bands at 479, 508, 622, and 627 cm^{-1} in going from curve (a) to curve (b). On this basis and on the basis of band widths, the latter set of bands mentioned above can be attributed to the monomer while

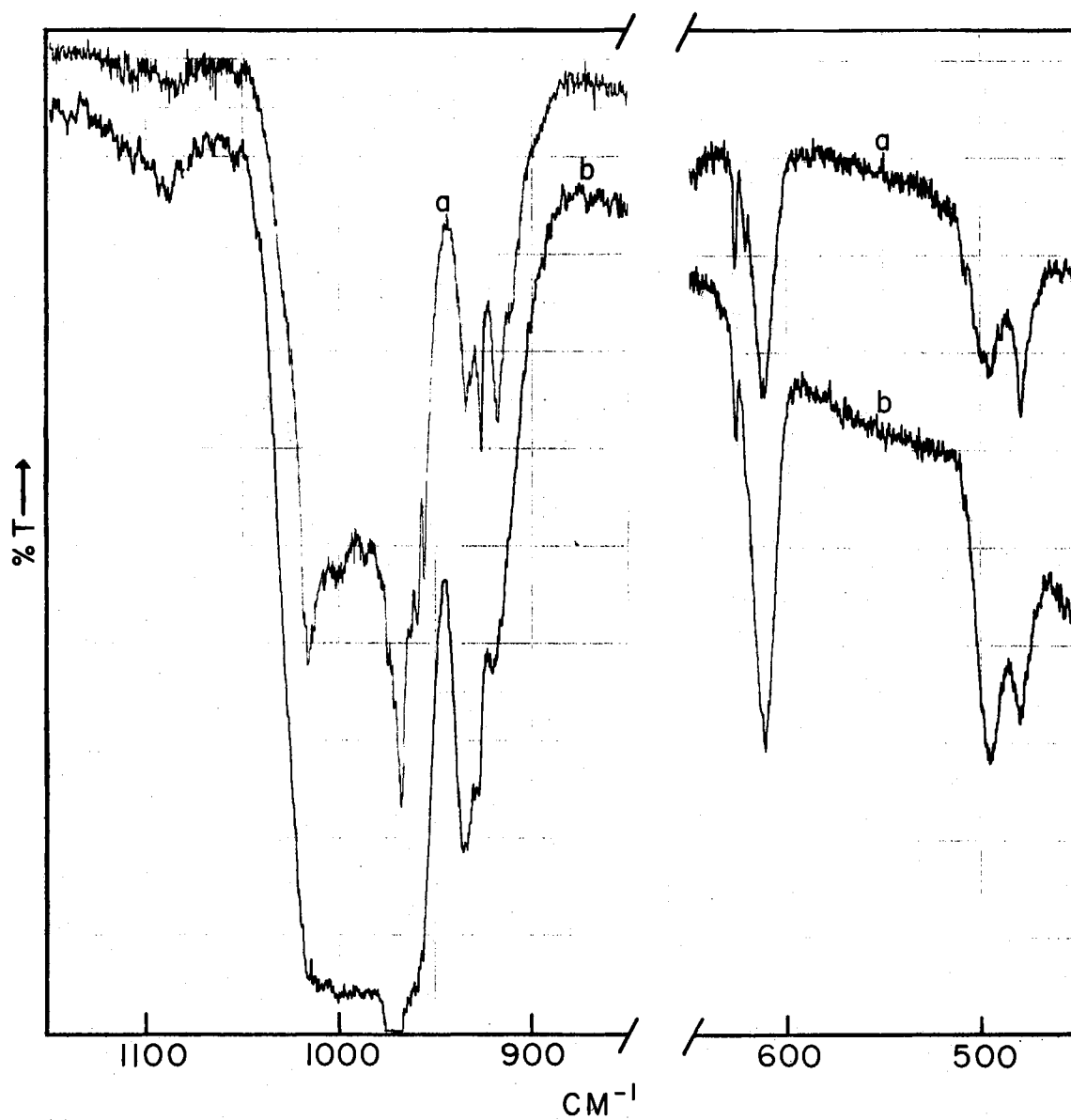


Figure 6. The Infrared Spectra of KClO_3 in Ar at 12°K with Different M/A Ratios: (a) Ar to KClO_3 ratio needed for near maximum isolation; (b) Ar to KClO_3 ratio well below that needed for maximum isolation

those at 495 and 611 cm^{-1} can be attributed to the dimer. The infrared spectrum of KClO_3 isolated in Xe appears in Figure 7. There is very little difference in the overall appearance of this spectrum as compared to that of KClO_3 isolated in Ar. There are, however, some slight shifts to lower frequency for most bands in changing the matrix material from Ar to Xe as can be seen more clearly in Table IV. Table IV lists the observed frequencies for KClO_3 isolated in both Ar and Xe along with their assignments.

The Raman frequencies which are listed in Table IV are from curves (a) and (b) of Figure 8. These curves, which represent the Raman spectra of KClO_3 isolated in both Ar and Xe in the 900-1020- cm^{-1} region, demonstrate the difficulty involved in achieving useful Raman results. With film thicknesses of about four times that for the sample of curve (a) in Figure 6, and with near maximum instrumental sensitivity, only the stronger scattering modes, i.e., symmetric modes, are detectable for the isolated KClO_3 samples of curves (a) and (b). Such results are similar to those observed for the matrix-isolated alkali-metal nitrates (8) in which only the ν_1 symmetric N-O stretching mode was observed by the Raman effect.

In the KClO_3 in Ar spectrum of curve (a), the strongest Raman feature has a maximum near 939 cm^{-1} which very likely corresponds to the 935- cm^{-1} infrared band and is, therefore, assigned to the ν_1 chlorate mode of the dimer. A weaker feature, appearing more or less as a wing on the low-frequency side of the 939- cm^{-1} band, apparently corresponds to the 917, 927- cm^{-1} infrared doublet and is assigned to the ν_1 chlorate mode of the monomer. The only other Raman feature in curve (a) appears very weakly near 969 cm^{-1} . This feature must correspond to the

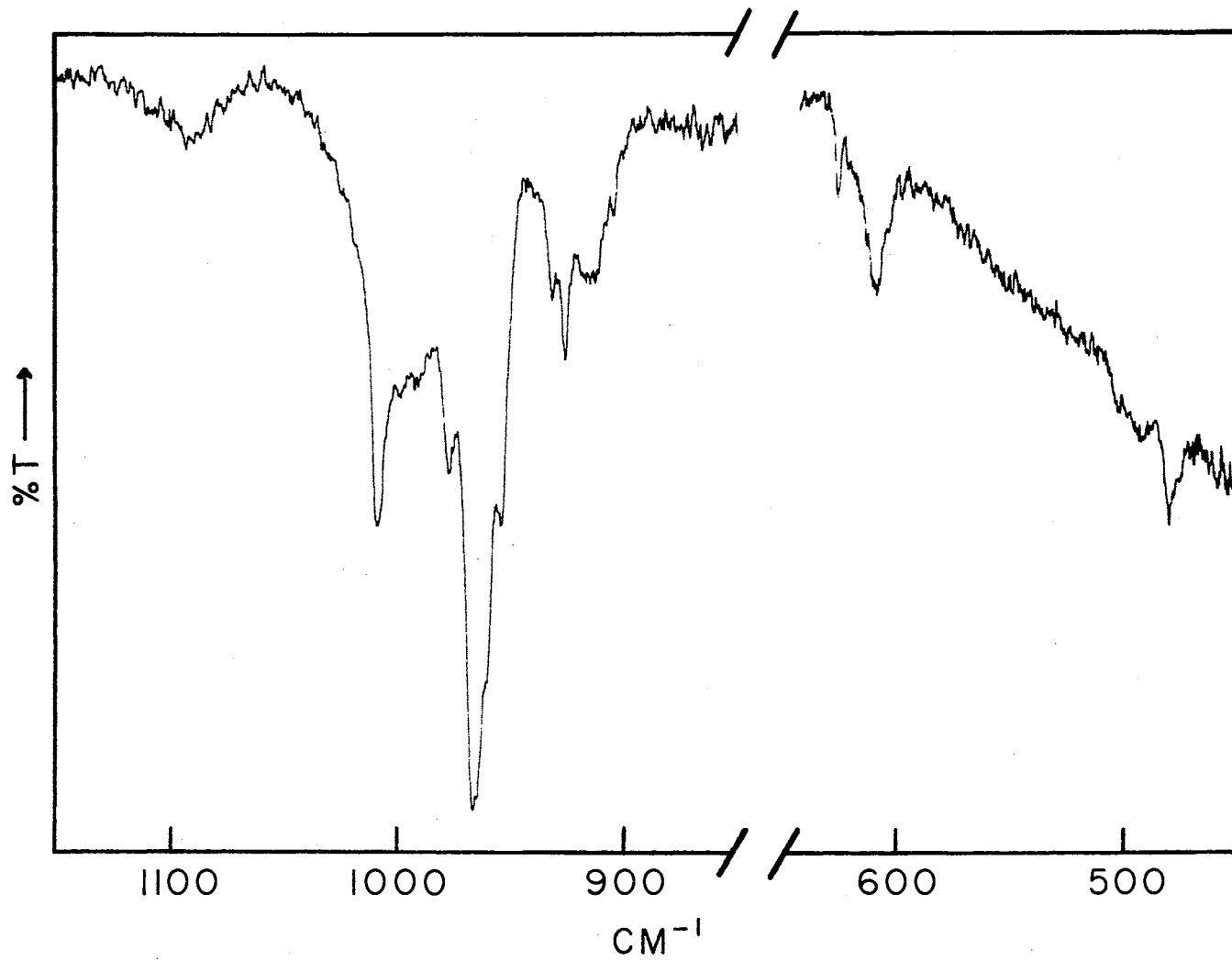


Figure 7. The Infrared Spectrum of KClO_3 Matrix Isolated in Xe at 12°K

TABLE IV
OBSERVED FREQUENCIES (CM^{-1}) FOR MATRIX-ISOLATED
VAPORS OF POTASSIUM CHLORATE^a

Infrared		Raman		Assignment ^b
Ar	Xe	Ar	Xe	
479	480			ν_{4a} Monomer
495	492			ν_4 Dimer
508	502			ν_{4b} Monomer
611	610			ν_2 Dimer
622 ^c	622			ν_2 Monomer
627	627			
	905			
917	915	927	927	ν_1 Monomer
927	926			
935	933	939	935	ν_1 Dimer
956	954			
959				
968	967	969	966	ν_{3a} Monomer
987	976			
	992			
1000	999			ν_3 Dimer
1017	1009			ν_{3b} Monomer
1088	1092			ν_3 ClO_2^d

^aFor relative intensities see appropriate figure.

^bModes involving predominately motion of the chlorate ion are numbered the same as for the "free" C_{3v} anion.

^cBrackets denote matrix site-splitting.

^dSee LiClO_3 results.

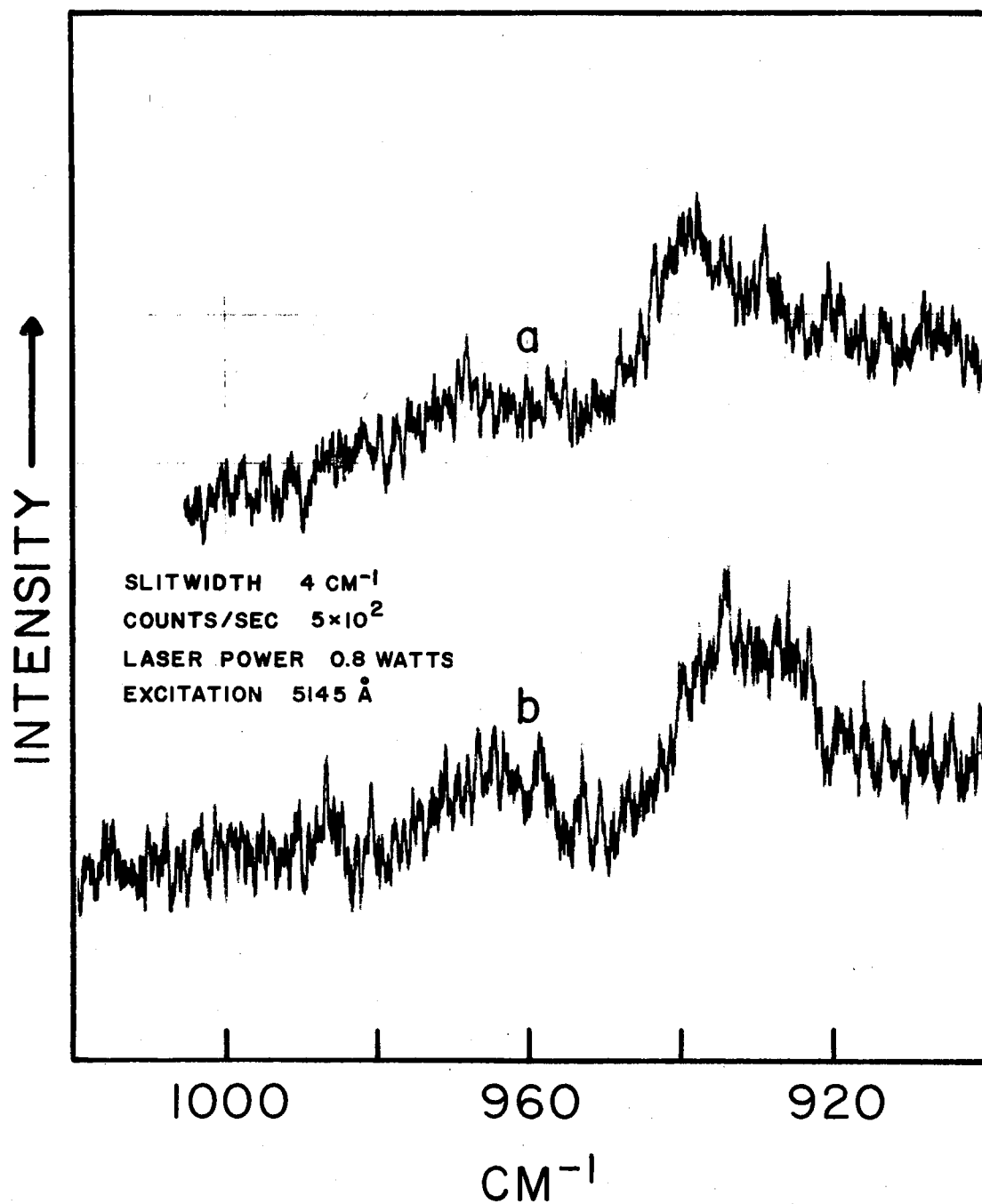


Figure 8. Raman Bands for ν_1 and ν_3 Modes of KClO_3 : (a) matrix isolated in Ar at 12°K; (b) matrix isolated in Xe at 12°K

very strong 968-cm^{-1} infrared band. Of the monomer features in the ν_1 and ν_3 region, only the 968 and 1017-cm^{-1} bands remain unassigned. Since ν_1 has been assigned, the 968 and 1017-cm^{-1} bands must correspond to the two components of the doubly degenerate ν_3 chlorate mode. The 968-cm^{-1} feature can further be interpreted as being the symmetric ν_3 component on the basis of the Raman results. The assignments for features in $900\text{-}1050\text{-cm}^{-1}$ of the KClO_3 in Xe spectrum can be made similarly with the aid of curve (b) in Figure 8 which exhibits the same general features as curve (a).

The assignments for the remaining features in the $450\text{-}650\text{-cm}^{-1}$ region of the spectrum in both Ar and Xe are easily made by comparing the observed frequencies with those of the unperturbed chlorate anion and with those of other members of the series. The bands in the $600\text{-}650\text{-cm}^{-1}$ region are assigned appropriately to the ν_2 chlorate mode of the monomer and dimer, while those around 500 cm^{-1} are likewise assigned to the ν_4 chlorate mode. Two components for the doubly degenerate ν_4 chlorate mode are observed for the monomer just as previously mentioned for the ν_3 mode.

It can be concluded from the well isolated case that the KClO_3 vapors consist of a mixture of monomers and dimers. The relative percentage of each of these species is difficult to estimate due to some rather unusual behavior associated with some of the infrared features. The ν_2 band of the dimer, for instance, dominates that of the monomer by almost an order of magnitude as can be observed in curve (a) of Figure 6. Other dimer features, however, do not exhibit such dominance over the corresponding monomer feature. In fact, in the ν_1 and ν_3 region the monomer features appear to dominate those of the dimer. This particular

behavior is not well understood. There is a much higher percentage of dimer relative to monomer for the thicker matrix samples such as are required for the Raman measurements. The additional dimers are apparently formed in the matrix through an inability to dissipate the added heat load caused by an increased deposition rate and film thickness.

Sodium Chlorate

The infrared spectrum of NaClO_3 isolated in Ar at 12°K appears in curves (a) and (b) of Figure 9. As was observed for KClO_3 , the very weak features near 1100 cm^{-1} in curve (a) indicate that only minor decomposition occurs on vaporization of NaClO_3 . Very little change in the spectrum is observed by further increasing the M/A ratio over that of curve (a), thus indicating the achievement of maximum isolation. With attention still directed to the $900\text{--}1100\text{-cm}^{-1}$ region, three strong band complexes at ca. 912 , 972 , and 1020 cm^{-1} and a band of moderate strength at ca. 1066 cm^{-1} , all with very sharp multiple band structure, can be observed in curve (a). The three lower frequency bands can most certainly be attributed to the NaClO_3 monomeric species on the basis of the diffusion results given in curve (c) and also by comparison with the results for the other members of the series. Although the 1066-cm^{-1} band appears also to belong to the same species, its origin is extremely puzzling as will be discussed later in this section. Curve (c), which represents the spectrum obtained after the sample of curve (a) was warmed to ca. 50°K , shows only some very slight remnants of the four features previously mentioned indicating the loss of isolation. The rather broad features appearing in curve (c), the most notable of which is centered at ca. 933 cm^{-1} , can be attributed to the formation of small

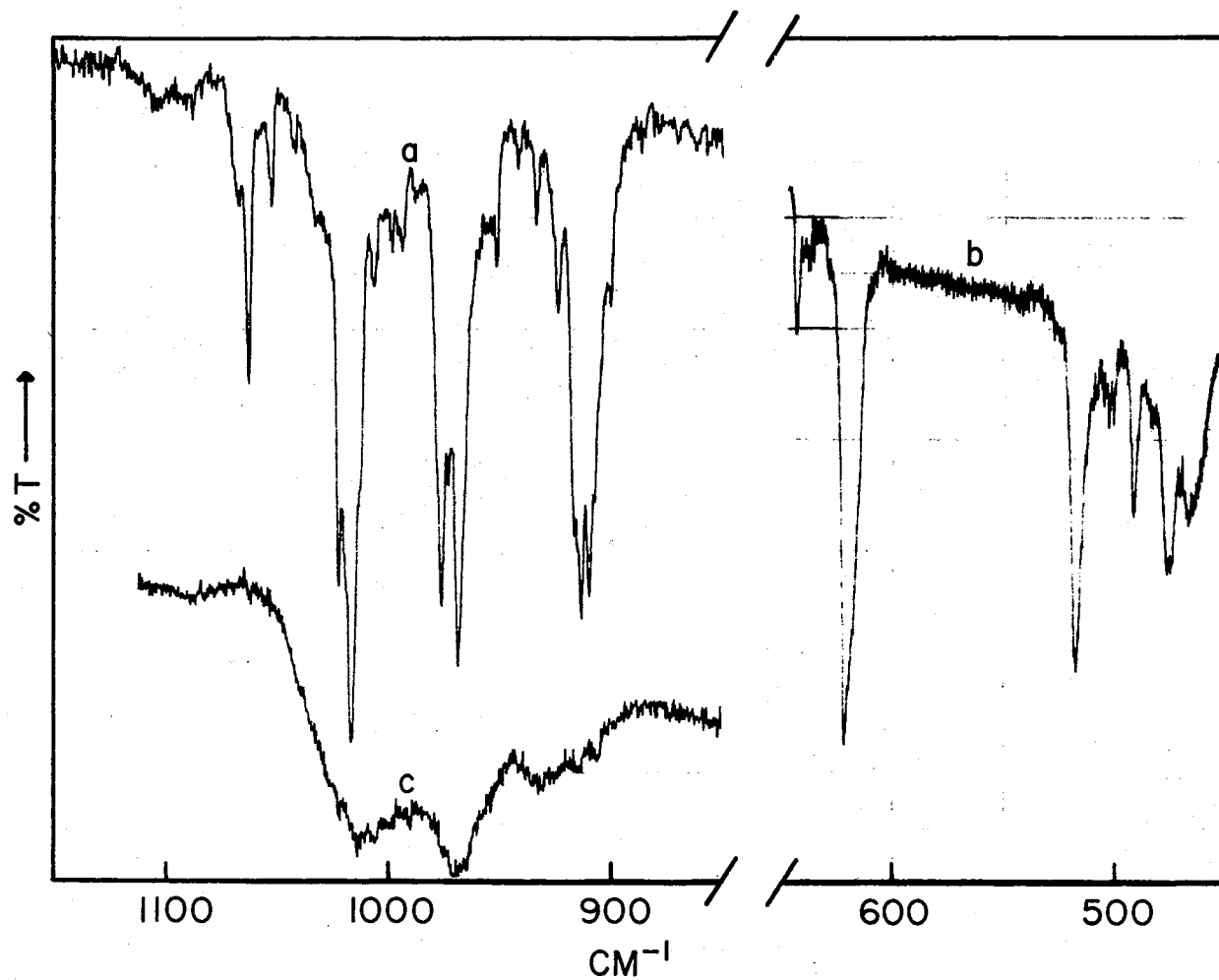


Figure 9. Infrared Spectrum of NaClO₃: (a) matrix isolated in Ar at 12°K; (b) matrix isolated in Ar at 12°K with a thickness of about three times that of curve (a); (c) matrix sample of curve (a) at 12°K after warming to ca. 50°K

NaClO_3 aggregates in the matrix following diffusion.

There are numerous weaker features observed in curve (a) whose origins are not too clear. Although some of these features are apparently due to polymeric species such as dimer, their identification is not as clear-cut as was observed for the KClO_3 case. Lowering the M/A ratio below that necessary for complete isolation apparently does not yield much further information which would be helpful in this respect. Perhaps by employing a more careful warm-up procedure than was presently utilized, it might be possible to better characterize the NaClO_3 polymeric species.

The multiple band structure for monomer features in curve (a) can be attributed to multiple trapping sites within the Ar matrix by comparison with the NaClO_3 in Xe spectrum which appears in Figure 10. A sharp reduction in band structure can be observed in the $900\text{-}1100\text{-cm}^{-1}$ region of curve (a) in the Xe matrix spectrum. Again, there are some slight shifts to lower frequency for most of the bands in changing the matrix material from Ar to Xe.

It can be concluded from curve (a) of Figures 9 and 10 that the monomer is most certainly the predominant species present in the NaClO_3 vapors. With this fact in mind, other monomer features can be identified in the $450\text{-}650\text{-cm}^{-1}$ region of the spectrum. At least three monomer bands are expected in this region by analogy with the KClO_3 results. Curve (b) of Figure 9, which represents a sample thickness of about three times that of curve (a), exhibits a considerably richer spectrum than one would expect. Bands observed at 518 and 622 cm^{-1} can be attributed to the monomer on the basis of their intensity. There are four weaker features appearing below the 518-cm^{-1} band, at least one of which

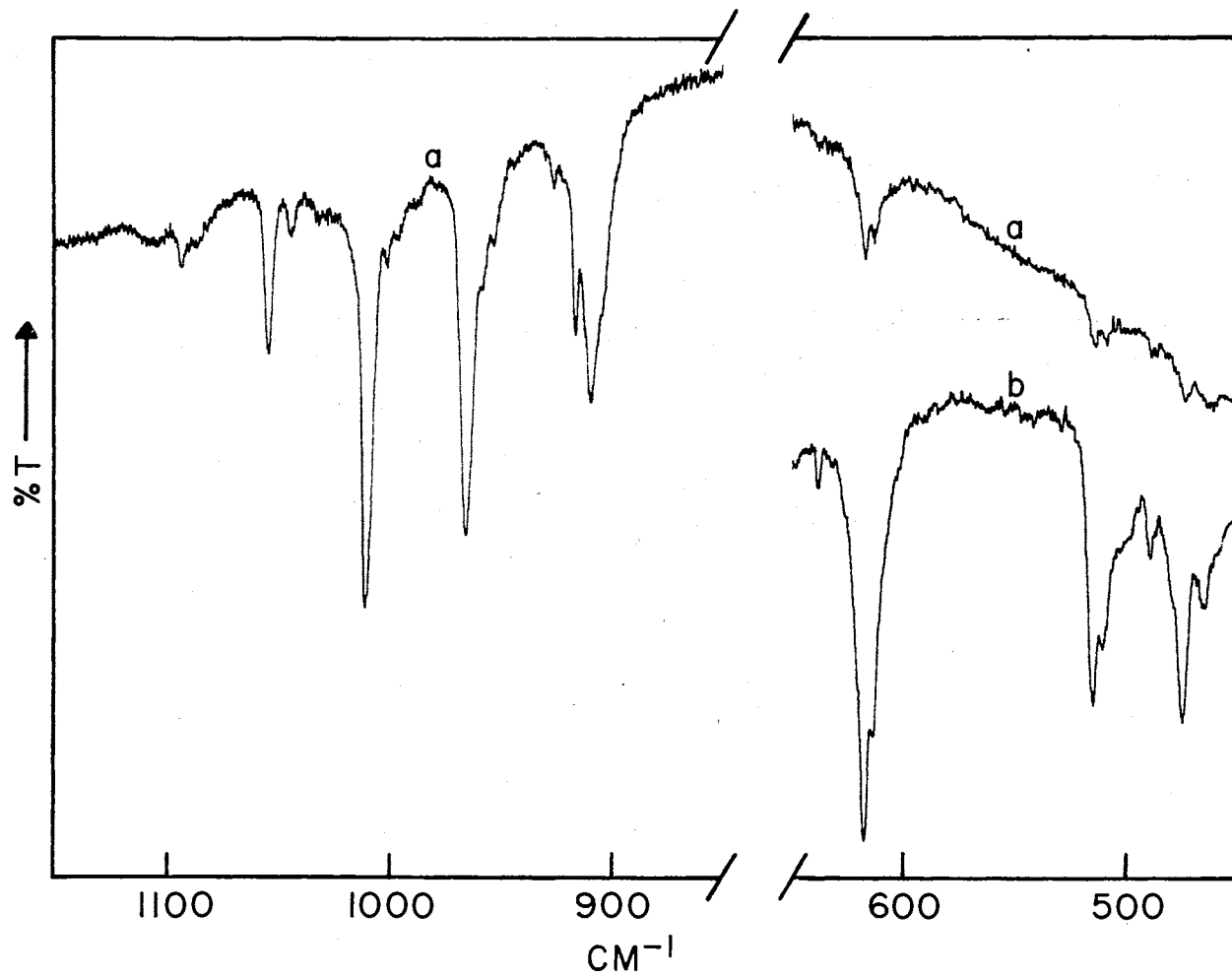


Figure 10. Infrared Spectrum of NaClO₃: (a) matrix isolated in Xe at 12°K;
(b) matrix isolated in Xe at 12°K with a thickness of about four
times that of curve (a)

must be attributable to the monomer. The 478-cm^{-1} band, which is the strongest of these features, appears to be the best choice. This is further confirmed by a comparison with the Xe matrix spectrum of curve (b) in Figure 10, which exhibits a corresponding feature of much greater prominence at 476 cm^{-1} . It was initially felt that one of the remaining features in the $450\text{-}500\text{-cm}^{-1}$ region might be due to the metal-chlorate stretching vibration of the monomer; however, data for LiClO_3 and subsequent calculations indicate that frequencies of this order are too high for such a mode in the NaClO_3 monomer. The 503-cm^{-1} band in the Ar matrix spectrum, which is observed to increase in intensity relative to the monomer features on reduction of the M/A ratio, can apparently be attributed to NaClO_3 dimer. The origin of the three remaining unassigned features in the $450\text{-}650\text{-cm}^{-1}$ region is unclear at this time.

The assignments for NaClO_3 monomer and dimer features, which appear in Table V, are made in a manner analogous to that discussed previously for isolated KClO_3 . The Raman spectrum of NaClO_3 isolated in Ar appearing in Figure 11 is again of great aid in the assignment of ν_1 and ν_3 chlorate modes. The conditions for which this spectrum was obtained are quite comparable to those utilized in obtaining the matrix Raman spectra of KClO_3 previously appearing in Figure 8. The ν_1 and ν_{3a} chlorate modes of the monomer are observed at 912 and 962 cm^{-1} , respectively, in the matrix Raman spectrum of Figure 11 along with the ν_1 chlorate mode of the dimer at 935 cm^{-1} . For this case the ν_1 modes of the monomer and dimer are sufficiently different in frequency so that each appears well resolved.

As previously pointed out, there are a number of extra features appearing in the infrared spectrum of matrix-isolated NaClO_3 which have

TABLE V
OBSERVED FREQUENCIES (CM^{-1}) FOR MATRIX-ISOLATED
VAPORS OF SODIUM CHLORATE^a

Infrared		Raman	Assignment ^b
Ar	Xe	Ar	
469	466		
478	476		ν_{4a} Monomer
493	491		
503	500		ν_4 Dimer
518	512		ν_{4b} Monomer
	516		
622	616		ν_2 Monomer
	619		
643	638		
900			
910	911	912	ν_1 Monomer
914			
924	918		
934	926	935	ν_1 Dimer
942	944		
952	953		
	958		
969	967	962	ν_{3a} Monomer
973			
976			
989	989		
994			
998	997		
1007	1001		
1017	1012		ν_{3b} Monomer
1023			
1035	1033		

TABLE V (Continued)

Infrared		Raman	Assignment ^b
Ar	Xe	Ar	
1042			
1053	1046		
1064	1056		
1068			
1091	1094		} $\nu_3 \text{ClO}_2^d$
1103	1106		

^aFor relative intensities see appropriate figure.

^bModes involving predominately motion of the chlorate ion are numbered the same as for the "free" C_{3v} anion.

^cBrackets denote matrix-splitting.

^dSee LiClO_3 results.

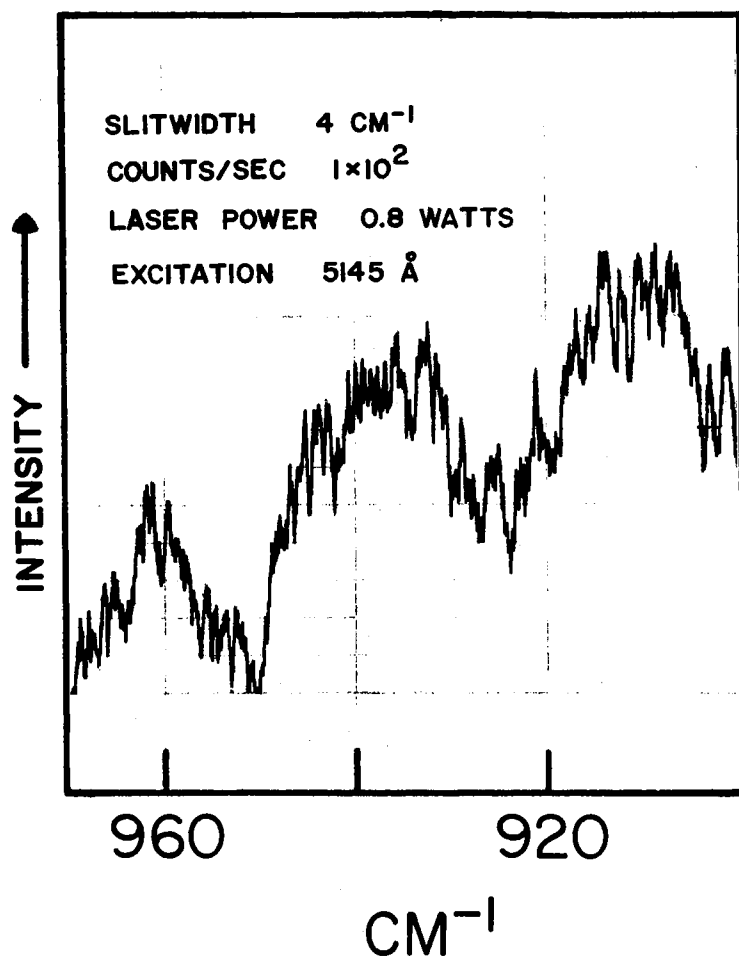


Figure 11. Raman Bands for ν_1 and ν_3 Modes of NaClO_3 Matrix Isolated in Ar at 12°K

no counterparts in the isolated spectra of KClO_3 or LiClO_3 . The most notable of these features is the 1064, 1068- cm^{-1} doublet in the Ar matrix spectrum and its Xe matrix counterpart at 1056 cm^{-1} . This particular feature behaves as though it belongs to the monomer species. If this were the case, the band would have to be due to a combination or overtone. A detailed analysis of the spectrum, however, has failed to yield a clear-cut assignment for the feature in this respect. One possibility would be a combination of one of the unobserved low-frequency bending modes with one of the chlorate stretching fundamentals. It is very likely on the basis of intensity that the band, if indeed a combination, involves some weak Fermi resonance with the high-frequency ν_3 component. Another possible explanation for the 1064, 1068- cm^{-1} doublet and certain of the other extra features in the infrared Ar matrix spectrum would be the existence of a second NaClO_3 monomeric species having a different bonding site for the sodium ion. This particular aspect will be further considered in the discussion section of this chapter.

A possible clue to the final resolution of the question concerning the origin of the 1064, 1068- cm^{-1} doublet may lie in the observation of Cl^{35} , Cl^{37} isotopic splitting for this feature. A band is observed at 1053 cm^{-1} in the Ar matrix spectrum which may well be due to the Cl^{37} isotope. The ratio of its intensity to that of the 1064, 1068- cm^{-1} feature appears to fit very closely the ratio of the Cl^{35} and Cl^{37} isotopes in natural abundance. The ca. 11- cm^{-1} splitting observed for these features also closely fits that expected for the Cl^{35} , Cl^{37} isotopic splitting of the ν_3 mode of the chlorate ion (6). The infrared Xe matrix spectrum with corresponding features at 1056 and 1046 cm^{-1} tends also to support the preceding statements.

Lithium Chlorate

The infrared spectrum of LiClO_3 isolated in Ar appears in curve (a) of Figure 12. Four strong band complexes can be observed at ca. 900, 966, 1020, and 1100 cm^{-1} in the $850\text{-}1150\text{-cm}^{-1}$ region of the spectrum. Curve (b), which represents the sample of curve (a) after warming to ca. 45°K , shows that the three lower-frequency band complexes have almost completely disappeared in favor of a rather broad absorption similar to that previously observed on warming the matrix samples of NaClO_3 and KClO_3 . The band complex near 1100 cm^{-1} apparently retains much of its original intensity but coalesces to a single band at 1090 cm^{-1} in going from curve (a) to curve (b). On comparing with the spectra of the other members of the series and also on the basis of the diffusion results of curve (b), the three lower-frequency bands can be attributed to the LiClO_3 monomeric species. By a similar argument it appears that the 1100-cm^{-1} band originates from some species other than LiClO_3 . The yellowish coloration of the LiClO_3 matrix films strongly suggests that considerable decomposition occurs on vaporization of the salt; therefore, it was felt that the 1100-cm^{-1} band must likely be due to a product of some mode of decomposition. This was further confirmed by the collection of a yellow volatile material in the liquid nitrogen trap following warm-up and the disappearance of the 1100-cm^{-1} band from the room temperature infrared scan of the remaining sample. The oxides of chlorine, ClO_2 and Cl_2O , appeared to be prime candidates for consideration as products of the decomposition since both are yellowish-red gases at room temperature. On examining the published infrared spectra for both compounds (39) (40), it was determined that ClO_2 is the major product of

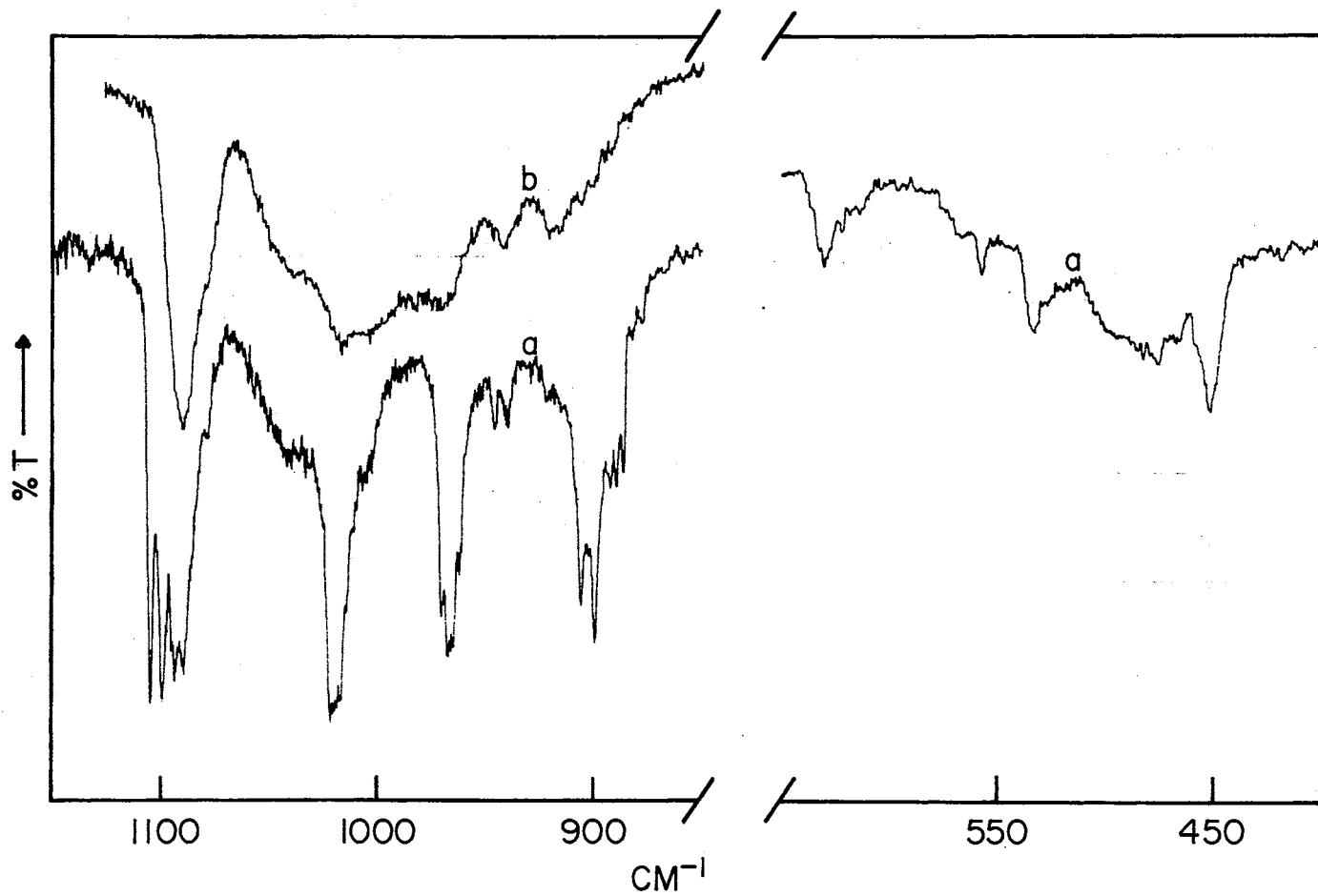


Figure 12. Infrared Spectrum of LiClO_3 : (a) matrix isolated in Ar at 12°K ; (b) matrix sample of curve (a) at 12°K after warming to ca. 45°K

decomposition.

The 1099, 1105 and 939, 946- cm^{-1} doublets and a single band at 448 cm^{-1} in curve (a) of Figure 12 correspond closely in position and intensity to the gas phase fundamentals of ClO_2 at 1110 (ν_3), 943 (ν_1), and 445 (ν_2) (39) and are apparently due to the ClO_2 isolated monomer. The 1089, 1094- cm^{-1} doublet and single features at 922 and 462 cm^{-1} can be attributed to a polymeric form of ClO_2 , probably dimer, on the basis of the diffusion results. The latter two features just mentioned can be seen much more clearly at 918 and 460 cm^{-1} in the LiClO_3 in Xe matrix spectrum of Figure 13 which shows a much higher percentage of ClO_2 relative to the LiClO_3 monomer. The assignments for the ClO_2 features are further confirmed by the infrared spectrum of ClO_2 isolated in Ar which appears in Figure 14. This spectrum was obtained quite unintentionally in an attempt to vaporize and isolate AgClO_3 for comparison with the alkali-metal chlorate results. It appears that AgClO_3 decomposes almost completely on vaporization as evidenced by the absence of any chlorate bands in the spectrum. Doublets are observed in the ClO_2 ν_1 and ν_2 fundamental regions which show rather clearly the presence of both ClO_2 monomer and dimer. The dominance of the 922 and 462- cm^{-1} features over those at 939 and 448 cm^{-1} indicates that the dimer is present in much greater abundance relative to monomer than was observed in the LiClO_3 matrix spectra. This fact along with the rather broad structureless feature observed in the ν_3 region indicates that ClO_2 sample of Figure 14 is not well isolated. Although the attempt to isolate AgClO_3 was unsuccessful, the experiment yielded some very useful information in regard to the identification and assignment of the bands due to decomposition products in the matrix-isolated spectra of LiClO_3 . It should be

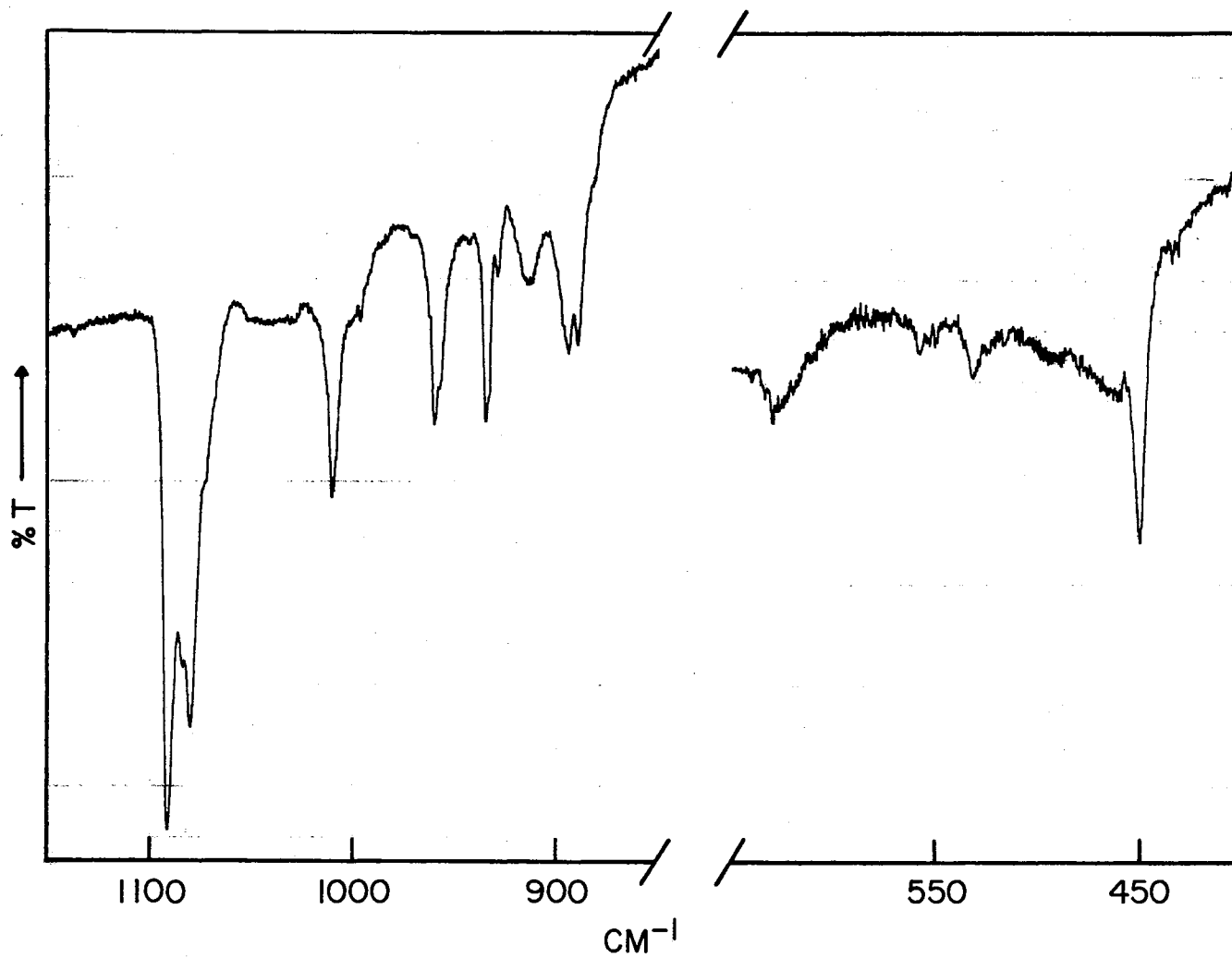


Figure 13. The Infrared Spectrum of LiClO_3 Matrix Isolated in Xe at 12°K .

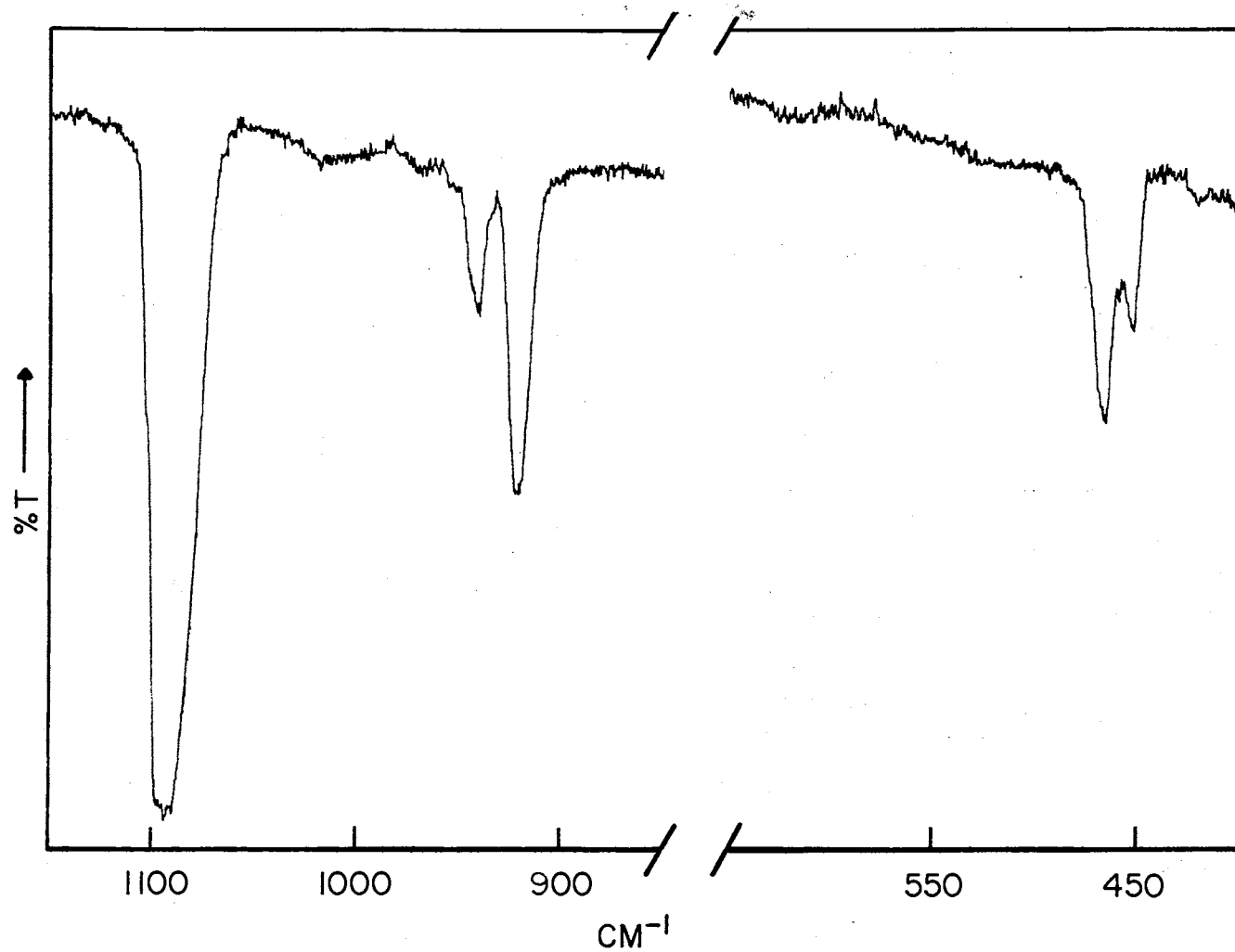


Figure 14. Infrared Spectrum of ClO₂ Matrix Isolated in Ar at 12^oK Generated by an Attempt to Vaporize AgClO₃

mentioned that the decomposition behavior of LiClO_3 may be linked to the extreme hygroscopic nature of this salt and an inability to get it completely dry prior to deposition. Some such factor must be involved since there is considerable variation in the amount of decomposition for a given deposition temperature as clearly exemplified by Figures 12 and 13.

Due to the high background signals apparently caused by fluorescence of ClO_2 and an inability to obtain a sufficient thickness of chlorate, the observation of Raman features for the LiClO_3 monomeric species was not possible. The Raman spectrum of the matrix-isolated vapors of LiClO_3 does, however, exhibit a feature in the $900\text{-}1000\text{-cm}^{-1}$ region. This feature appears at 944 cm^{-1} in the Ar matrix spectrum, as can be seen in Figure 15, and must quite obviously be due to the ν_1 mode of the ClO_2 monomer. The intensity of this band is somewhat surprising in view not only of the previously mentioned problem concerning the background but also the thickness of the ClO_2 in the matrix samples, which for the most part was quite moderate in comparison to that required in obtaining Raman signals for the matrix-isolated Na and K chlorates. The ν_1 mode of ClO_2 was, in fact, detectable in samples comparable in thickness to that of curve (a) in Figure 12. Figure 15 represents a sample of about two and one-half times this thickness. Although of no particular pertinence to the present problem, it might be mentioned that much of the intensity observed for the 944-cm^{-1} band in Figure 15 may well be derived from a resonant Raman scattering effect.

It can be concluded from the $850\text{-}1050\text{-cm}^{-1}$ region of the matrix spectra in Figures 12 and 13 that the LiClO_3 monomer is the major constituent, excluding decomposition products, of the vapors above the salt.

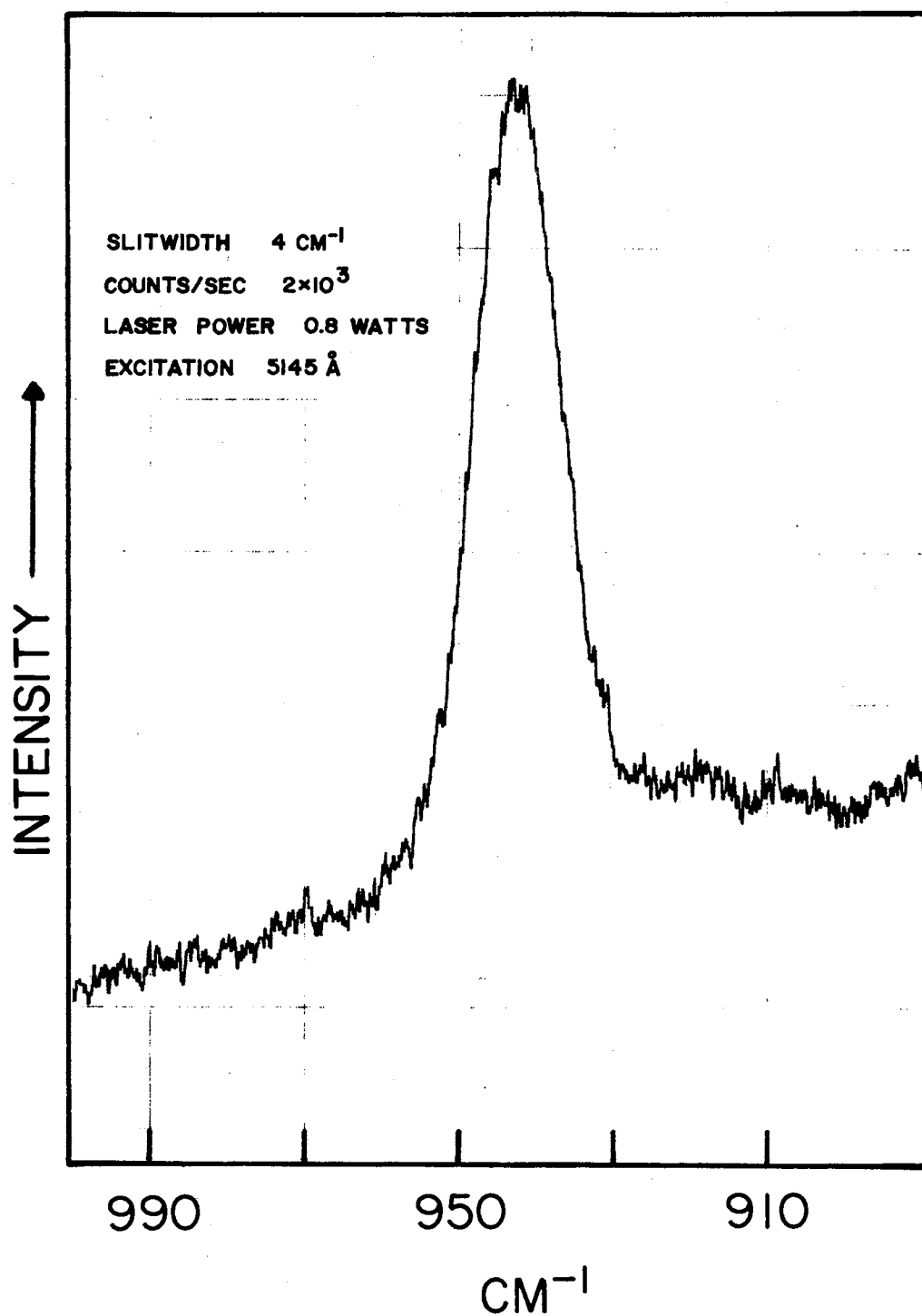


Figure 15. The $890\text{--}1000\text{-cm}^{-1}$ Region of the Raman Spectrum for the LiClO_3 Vapors Matrix-Isolated in Ar at 12°K

Having determined the bands in the infrared matrix spectra which are due to decomposition permits other LiClO_3 monomer features in the 450-650- cm^{-1} region to be identified. With these facts in mind, the bands appearing at 630, 557, 533, and 481 cm^{-1} in curve (a) of Figure 12 are, then, quite obviously due to the LiClO_3 monomer. The 481- cm^{-1} band is quite weak and is observed much more clearly in the spectra of the thicker samples.

Table VI lists the observed infrared and Raman frequencies for the matrix-isolated vapors of LiClO_3 along with the assignments for the majority of these bands. The assignments for the LiClO_3 monomer features with the exception of those at 557 and 533 cm^{-1} can easily be made just by comparison with the NaClO_3 and KClO_3 results. The uncertainty over the assignment of the 557 and 533- cm^{-1} bands comes from the fact that an extra feature is observed in this region which is apparently due to the Li-ClO_3 cation-anion stretching mode. Since the high-frequency component of the doubly degenerate ν_4 chlorate mode is also expected in this region, it became necessary to rely upon the normal coordinate calculations in order to help distinguish between these two features. On the basis of these calculations, the 557 and 533- cm^{-1} bands are assigned as the ν_{4b} and $\nu_{\text{Li-ClO}_3}$ modes, respectively.

It should be mentioned that the weaker features observed on the low-frequency side of the ν_1 chlorate mode in the Ar matrix spectrum of curve (a) in Figure 12 are apparently due to further matrix site-splitting of this mode, since there is little evidence for these features in the Xe matrix spectrum of Figure 13. One also sees very little evidence for extra features in the infrared matrix spectra which would be indicative of the presence of dimers or other polymer species in the vapors above

TABLE VI

OBSERVED FREQUENCIES (CM^{-1}) FOR MATRIX-ISOLATED
VAPORS OF LITHIUM CHLORATE^a

Infrared		Raman	Assignment ^b
Ar	Xe	Ar	
448	445		ν_2 ClO_2 Monomer
462	460		ν_2 ClO_2 Dimer
481	479		ν_{4a} LiClO_3 Monomer
533	531		$\nu_{\text{Li-ClO}_3}$ LiClO_3 Monomer
557	554		ν_{4b} LiClO_3 Monomer
630	630		ν_2 LiClO_3 Monomer
878			}
883			
887			
890			
893			
900	893		ν_1 LiClO_3 Monomer
907	897		
922	918		ν_1 ClO_2 Dimer
939	932		}
946	938		
962		944	ν_1 ClO_2 Monomer
966	963		ν_{3a} LiClO_3 Monomer
970			
1004	1000		
1020	1014		ν_{3a} LiClO_3 Monomer
1036			
1042			
1078			

TABLE VI (Continued)

Infrared		Raman	Assignment ^b
Ar	Xe	Ar	
1089 } 1094 }	1084 } 1088 }		ν_3 ClO ₂ Dimer
1099 } 1105 }	1095		ν_3 ClO ₂ Monomer

^aFor relative intensities see appropriate figure.

^bModes involving predominately motion of the chlorate ion are numbered the same as for the "free" C_{3v} anion.

^cBrackets denote matrix site-splitting.

the salt.

Discussion

On the basis of the splitting of the degenerate ν_3 and ν_4 modes, it can be concluded that the C_{3v} chlorate symmetry has been lowered in the $MClO_3$ monomers either by unidentate or bidentate coordination of the metal ion through the oxygen atoms. Distinguishing between unidentate and bidentate coordination should in principle be easily determined from the infrared and Raman spectra; however, such a distinction for the $MClO_3$ monomers would require a more complete set of data than is presently available.

Of the nine possible vibrational modes, the six primarily involving motions of the anion would be very similar in both models while the three involving the metal coordination would differ considerably. The latter three modes just mentioned would consist of two bends and one stretch for the unidentate model while for the bidentate model the number of bending and stretching modes would just be reversed. The bending modes would be expected at very low frequency, probably well below 200 cm^{-1} , while the M-O stretching modes would be expected at somewhat higher frequencies depending on the mass of the cation. Since observation of Raman features for these modes is most certainly out of the question, the far infrared must be relied on heavily for the possible resolution of the problem concerning metal coordination in the $MClO_3$ monomers. Although the infrared instrument utilized for this investigation has a lower limit of 200 cm^{-1} , its reliability below 300 cm^{-1} is somewhat questionable, and for this reason one could at most expect to observe the M-O stretching modes. The $LiClO_3$ monomer is, however, the only member of the $MClO_3$

series for which such a mode has been observed.

Even though the observation of a single band at 533 cm^{-1} which is attributable to M-O stretching might tend to favor unidentate coordination, such data is inconclusive for the LiClO_3 monomer since a weakly absorbing symmetric M-O stretch for the bidentate case might easily be overlooked for the film thicknesses investigated. It might be mentioned that the very thick matrix films utilized in the Raman investigation of the NaClO_3 and KClO_3 monomers were examined closely in the far infrared region for M-O stretching modes without success. Calculations based on the LiClO_3 data, as will be presented later, indicate that this mode probably lies below 300 cm^{-1} for both NaClO_3 and KClO_3 .

There is one piece of evidence from the Raman spectra of the NaClO_3 and KClO_3 monomers which would cause one to lean in favor of unidentate structure. This evidence happens to be the observation of the low-frequency component of the ν_3 chlorate mode in the Raman spectra which, as mentioned before, would tend to indicate that it is the more symmetric component. From normal coordinate calculations on the unidentate and bidentate models of the alkali metal nitrates (41)(42), it has been ascertained that the symmetric ν_3 component is of lower frequency than the asymmetric component in the unidentate model but is the higher of the two in the bidentate model. It is not unreasonable to expect a similar sort of behavior for the alkali-metal chlorates.

In the earlier discussion of the NaClO_3 results, the presence of a second monomeric species was given as one possible explanation for the $1064, 1068\text{-cm}^{-1}$ infrared doublet observed in the Ar matrix spectrum of Figure 9. Since the metal cation for the "major" monomeric species has been determined to coordinate through the oxygen atoms, a second species,

if indeed it exists, would likely involve metal coordination through the chlorine atom. Such coordination would probably leave the C_{3v} symmetry of the chlorate anion intact; thus, one would expect to see only four vibrational frequencies for the chlorate portion of the molecule. These frequencies could be shifted considerably from the "free anion" values since this type of metal coordination is expected to strengthen the bonding in the chlorate anion. It would not be unreasonable, then, to speculate that other unassigned features at 924, 643, and 491 cm^{-1} in the matrix spectrum of Figure 9 might also be due to the second monomeric species. Although this aspect requires considerably more study before any definite conclusion can be reached, it will not be pursued any further in the present investigation.

A list of observed frequencies for the MClO_3 monomers isolated in both Ar and Xe appears in Table VII, and it is interesting to note from this table the frequency trends for the various modes. The ν_1 mode is observed to increase through the series from Li to K while ν_2 , both components of ν_3 , and the lower-frequency component of ν_4 remain essentially constant. The higher-frequency component of ν_4 exhibits the reverse trend to that of ν_1 , as it is observed to decrease through the series.

One can also see quite clearly from Table VII the splitting patterns for the degenerate ν_3 and ν_4 modes. It was mentioned in the introductory chapter that the magnitudes of such splittings can roughly serve as a measure of the cation polarization of the anion. The splitting of ν_4 , which is observed to decrease through the series from Li to K, apparently reflects the diminishing trend in the polarizing powers for the alkali-metal cation series. The splitting of ν_3 , surprisingly enough, remains almost constant throughout the whole MClO_3 monomer series. This behavior

TABLE VII

OBSERVED FREQUENCIES (CM^{-1}) FOR THE ALKALI-METAL
CHLORATE MONOMERS ISOLATED IN
BOTH ARGON AND XENON^a

M^+	Matrix	ν_1	ν_2	ν_{3a}	ν_{3b}	ν_{4a}	ν_{4b}	$\nu_{M-\text{ClO}_3}$
Li	Ar	^b $\left\{ \begin{array}{l} 900 \\ 907 \end{array} \right.$	630	$\left\{ \begin{array}{l} 962 \\ 966 \\ 970 \end{array} \right.$	1020	481	557	533
	Xe	$\left\{ \begin{array}{l} 893 \\ 897 \end{array} \right.$	630	963	1014	479	554	531
Na	Ar	$\left\{ \begin{array}{l} 910 \\ 914 \end{array} \right.$	622	$\left\{ \begin{array}{l} 969 \\ 973 \\ 976 \end{array} \right.$	$\left\{ \begin{array}{l} 1017 \\ 1023 \end{array} \right.$	478	518	---
	Xe	911	$\left\{ \begin{array}{l} 616 \\ 619 \end{array} \right.$	967	1012	476	$\left\{ \begin{array}{l} 512 \\ 516 \end{array} \right.$	---
K	Ar	$\left\{ \begin{array}{l} 917 \\ 927 \end{array} \right.$	$\left\{ \begin{array}{l} 622 \\ 627 \end{array} \right.$	968	1017	479	508	---
	Xe	$\left\{ \begin{array}{l} 915 \\ 926 \end{array} \right.$	$\left\{ \begin{array}{l} 622 \\ 627 \end{array} \right.$	967	1009	480	502	---

^aModes involving predominately motion of the chlorate ion are numbered the same as for the "free" C_{3v} anion.

^bBrackets denote matrix site-splitting.

is completely unexplained particularly if one recalls the results given in Chapter I for the ν_3 splittings in MNO_3 monomer series. The normal coordinate calculations, which will be presented in the next chapter, appear to shed some light on this rather unexpected result for ν_3 in the chlorates.

There are some rather interesting observations in regard to the intensity behavior for several of the chlorate modes in the monomer series, which require some mention. For instance, the higher-frequency infrared component for both ν_3 and ν_4 is observed in both the LiClO_3 and NaClO_3 monomers to have a greater intensity than the lower-frequency component, while just the opposite is observed for the KClO_3 monomer. Very little can be said about this intensity reversal for KClO_3 other than to mention that some sort of vibronic effect is probably involved. The increasing trend in the infrared intensity of the ν_1 mode through the series in going from K to Li is also worthy of note. This behavior can apparently be explained in terms of the unidentate model as an increase in the decoupling of the associated Cl-O bond stretching from the stretching motion of the remainder of the anion as the cation is changed through the series from K to Li.

Matrix-Isolated Lithium Nitrate

The present matrix-isolation study involving LiNO_3 in Ar was initiated in an effort to refine the previous infrared results reported for the LiNO_3 monomer in CO_2 and CCl_4 matrices (8). Much thicker matrix films than were obtained in the original work were prepared in hope of gaining some new information regarding the weak ν_4 degenerate planar bending mode. It was further hoped that a more careful examination of

the 200-700-cm⁻¹ region might lead to the observation of the metal-nitrate stretching frequency which was not observed in the original work.

The infrared spectrum of LiNO₃ isolated in Ar at 12^oK appears in Figure 16. Curve (a) of this figure represents a well isolated sample of moderate thickness while curve (b) represents a sample with a thickness of about five times that of curve (a). The two components of the doubly degenerate asymmetric stretching mode appear very prominently at 1264 and 1524 cm⁻¹ in curve (a). One can further see in curve (a) a band at 528 cm⁻¹ which obviously must be the metal-anion stretching mode. It should be noted that this interior mode has an intensity greater than the ν_2 out-of-plane bending mode, which appears at 817 cm⁻¹, but somewhat less than that observed for either of the ν_3 components. Another very interesting fact is the relatively small frequency difference (5 cm⁻¹) that is observed when comparing the M-O stretching modes for the LiNO₃ and LiClO₃ monomers.

If attention is now shifted to curve (b), the two components of ν_4 can be identified. One component appears with reasonable intensity (ca. 1/3 that of ν_2) at 765 cm⁻¹ and is assigned with little chance of error. The other component is more difficult to identify since there are four weaker features which appear regularly at 692, 736, 747, and 783 cm⁻¹. The 747-cm⁻¹ feature is known to result from aggregates, (LiNO₃)_n, while the 783-cm⁻¹ value falls outside the range normally expected for a nitrate ν_4 mode. The choice is thus narrowed to the bands at 692 and 736 cm⁻¹. The 692-cm⁻¹ feature would be the preferred value if ν_4 were to behave similarly to ν_3 and split uniformly about the solid state value (735 cm⁻¹). The 736-cm⁻¹ feature, however, would appear to be more in line with the ν_4 results which have been observed for the MClO₃ monomer

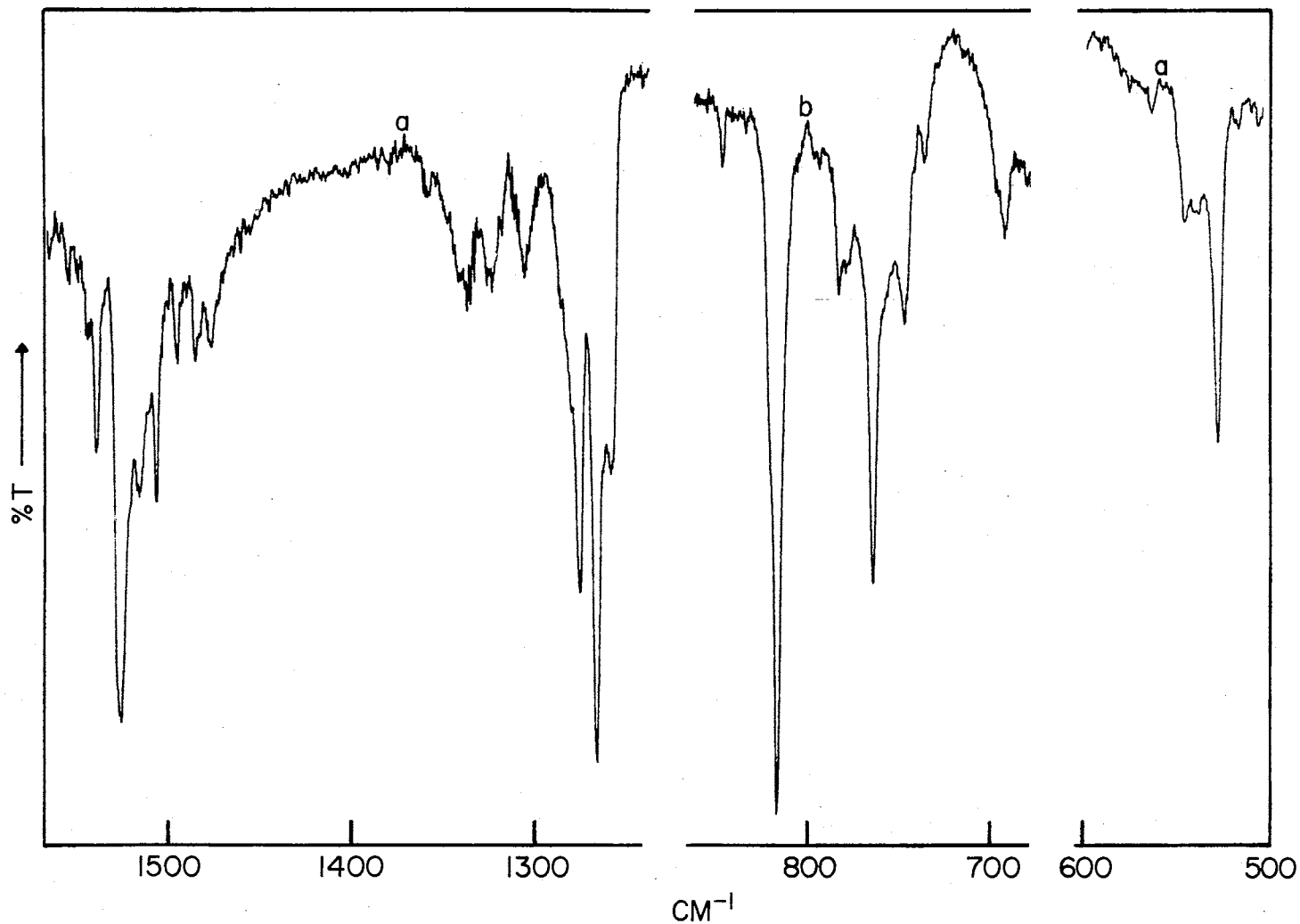


Figure 16. The Infrared Spectrum of LiNO_3 : (a) matrix isolated in Ar at 12°K ; (b) matrix isolated in Ar at 12°K with a thickness of about five times that of curve (a)

series. It should be recalled that the lower-frequency ν_4 component for $MClO_3$ monomers remained nearly invariant at approximately the solid state value (480 cm^{-1}) while the higher-frequency component was observed to increase in frequency through the series from K to Li. The 736-cm^{-1} feature is, thus, the preferred choice for the second component of ν_4 . It should be noted that the 765-cm^{-1} component is almost an order of magnitude more intense than the 736-cm^{-1} feature.

The ν_1 symmetric stretching mode although not presented in Figure 16 was observed at 1011 cm^{-1} . The observed frequencies for the $LiNO_3$ monomer matrix isolated in Ar are compiled in Table VIII.

TABLE VIII
THE OBSERVED INFRARED FREQUENCIES FOR THE
LITHIUM NITRATE MONOMER MATRIX
ISOLATED IN ARGON

Mode	Frequency (cm^{-1})
ν_1	1011
ν_2	817
ν_{3a}	1264
ν_{3b}	1524
ν_{4a}	736
ν_{4b}	765
ν_{Li-NO_3}	528

Alkali-Metal Nitrate Glass

Transition Temperatures

Glassy films of LiNO_3 , NaNO_3 , KNO_3 , and TlNO_3 were prepared by vapor deposition at 12°K , and estimates of T_g for these films were made from a measurement of glass-crystallization temperatures. Once the glassy nitrate film had been prepared, the typical experimental procedure consisted of warming the film at a rate of ca. $1^\circ\text{K}/\text{min.}$ with each film subsequently exhibiting an irreversible conversion to the crystalline solid. The temperatures for this glass-crystallization process were accurately established by monitoring the infrared-active ν_2 nitrate mode and observing the temperature at which significant spectroscopic changes occurred, i.e., frequency shift and/or half-bandwidth reduction. Figure 17, which shows the ν_2 band of LiNO_3 at the glass-crystallization temperature, represents the typical results observed for the entire nitrate series. The ν_2 band of the glass is shown in curve (a) of Figure 17 at 254°K , the temperature at which the film just begins to crystallize as evidenced by the appearance of the 838-cm^{-1} feature. The heating rate of $1^\circ\text{K}/\text{min.}$ was sharply reduced at this point. After five minutes with the temperature still held at 254°K , considerable conversion of the glass to the crystalline form had occurred as shown by curve (b). Curve (c) shows that the conversion was essentially complete after fourteen minutes and with a final temperature of 255°K .

The glass-crystallization values for the present study which were found to be reproducible to $\pm 2^\circ\text{K}$, along with the extrapolated values of Angell and Helphrey (10), appear in Table IX for comparative purposes. Before making such a comparison, however, it should be pointed out that

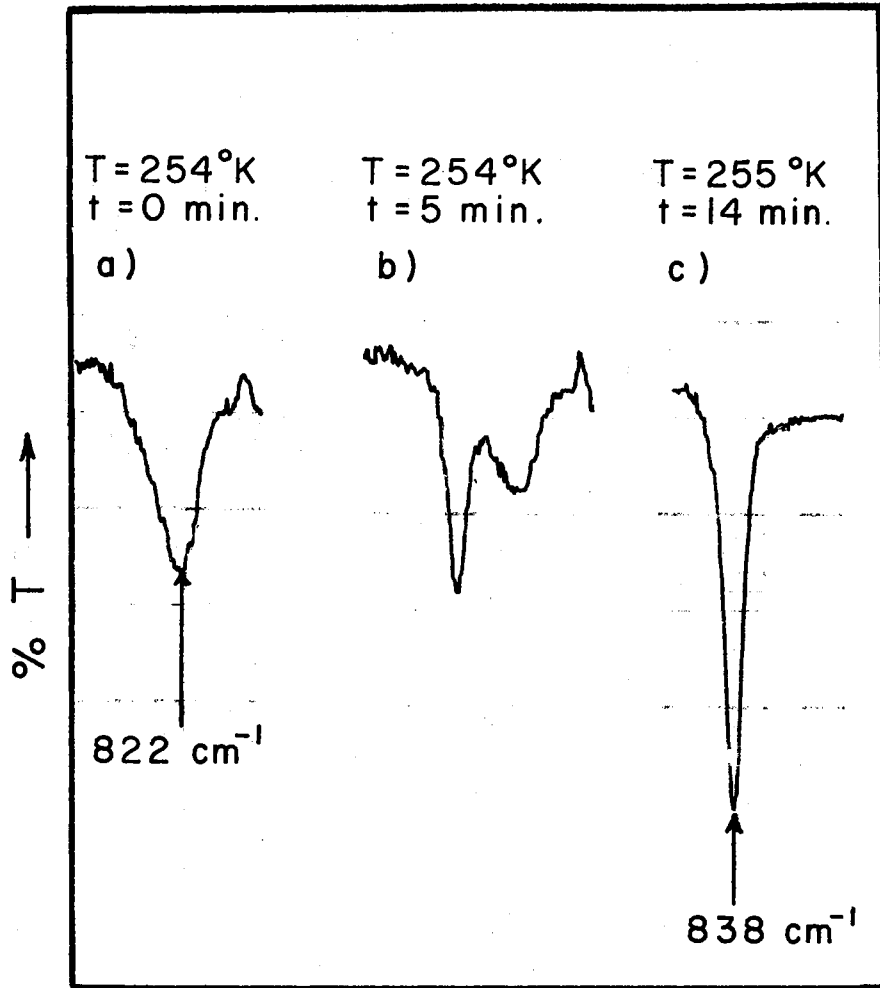


Figure 17. Infrared ν_2 Band of LiNO_3 at the Glass-Crystallization Temperature: (a) glass; (b) mixture of glass and crystal; (c) crystal

the glass transition temperature experienced by vapor-deposited glassy water (35) (43), which agrees closely with the extrapolated value from binary salt-water solutions (44), is some 20° - 30° K below the T_g value predicted from thermodynamic data (45), and that this discrepancy is not clearly understood. Angell and Sare (44) suggested, as a plausible explanation, the possibility of different short-range ordering for the vapor-deposited glassy water from that which water adopts upon cooling.

TABLE IX
NITRATE GLASS TRANSITION TEMPERATURES^a

Salt	T_g ($^{\circ}$ K) ^b	T_g ($^{\circ}$ K) ^c
LiNO ₃	253	228
NaNO ₃	224	226
KNO ₃	208	225
RbNO ₃		218
CsNO ₃		212
TlNO ₃	175	

^aAverage from two runs on each nitrate.

^bGlass-crystallization temperature determined in the present study.

^c"Experimental" glass transition temperatures from the work of Angell and Hephrey (10).

Table IX shows the T_g values of NaNO_3 for the two studies to be in good agreement, but the close similarity ends at that point. The extrapolated T_g values show only a spread of 16°K for the entire alkali-metal nitrate series and a spread of only 3°K from LiNO_3 to KNO_3 , whereas the glass-crystallization T_g values from the present study exhibit a definite cation-dependent trend with a spread of 45°K for the latter interval. Such a variation of T_g with alkali-metal cation size is consistent with expectations based on crystal energies and Debye θ values. The T_g value shown for TlNO_3 should be lower than for a number of the alkali-metal nitrates (10).

It was mentioned previously that attempts would be made to extend the determination of glass transition temperatures to the vapor-deposited alkali-metal chlorate thin films. The structure of these films appears to be glassy in nature; however, initial attempts at warming these films has failed to yield any clear-cut transition temperature like those observed for the alkali-metal nitrates.

CHAPTER IV

NORMAL COORDINATE CALCULATIONS

MClO_3 Monomers

A reasonable model for the MClO_3 monomers was established from an analysis of the experimental vibrational data in the previous chapter. Normal coordinate calculations were performed on this model in an effort to obtain a better understanding of the perturbing forces and their effects on the bonding in the monomer. These calculations yielded not only reasonable estimates of changes in the force field relative to the uncomplexed C_{3v} anion but also gave some insight into the rather unusual splitting behavior observed for the ν_3 mode in the MClO_3 monomer series.

The calculational procedure which was followed is very similar to that used by Brintzinger and Hester in their calculations involving oxyanion metal complexes (41). Briefly this procedure consists of finding a force field which satisfactorily reproduces the "free anion" frequencies. This field is then perturbed in ways corresponding to metal binding and oxyanion polarization. Due to the amount of vibrational data accumulated for the MClO_3 monomers, it was felt one could proceed a step further by attempting to fit a set of force constants to the observed frequencies. These calculations, incidently, were carried out by computer utilizing programs written by Overend and Scherer (46).

The Model and the Force Field

The model that was chosen for the $MClO_3$ monomers consisted of a unidentate structure with the metal bound linearly through one oxygen atom as depicted in Figure 18. This model is not unique since a bent structure would probably fit the observed data just as well. The structural parameters for the chlorate portion of the molecule were transferred from the "free anion" (6) and were assumed to be unchanged by coordination. This assumption can be made since changes in force constants produced by coordination, particularly those involving bond stretching, are expected to be of much greater significance than any geometrical change. The structural parameters used for the chlorate ion were $r_1 = r_2 = R = 1.477 \overset{\circ}{\text{A}}$ and $\beta_1 = \beta_2 = \alpha = 107.1^\circ$ (6). The M-O bond distances of $1.59 \overset{\circ}{\text{A}}$ and $2.0 \overset{\circ}{\text{A}}$ for the respective monomers of $LiClO_3$ and $NaClO_3$ were transferred from the corresponding distances in LiO (47) and NaO (48). The K-O bond distance of $2.32 \overset{\circ}{\text{A}}$ used for the $KClO_3$ monomer was an estimated value.

The model of the $MClO_3$ monomer which appears in Figure 18 possesses only a single plane of symmetry and, thus, belongs to the C_s molecular point group. The nine fundamental modes are distributed as $6A'$ and $3A''$ vibrations. Symmetry coordinates were constructed from the nine internal coordinates in order to take advantage of the molecular symmetry and are given as follows:

for A' ,

$$S_1 = \Delta(r_1 + r_2)/2^{\frac{1}{2}} \quad (ClO_2 \text{ symmetric stretch}),$$

$$S_2 = \Delta R \quad (Cl-O^* \text{ stretch}),$$

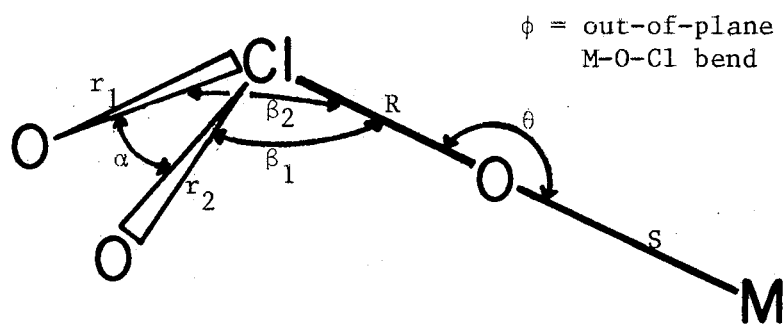


Figure 18. Geometry and Internal Coordinates for the MClO_3 Monomer

$$\begin{aligned}
S_3 &= \Delta\alpha && (\text{ClO}_2 \text{ scissor}), \\
S_4 &= \Delta(\beta_1 + \beta_2)/2^{1/2} && (\text{ClO}_2 \text{ wag}), \\
S_5 &= \Delta S && (\text{M-O}^* \text{ stretch}), \\
S_6 &= \Delta\theta && (\text{Cl-O}^*\text{-M deformation}), \\
\text{for } A'', \\
S_7 &= \Delta(r_1 - r_2)/2^{1/2} && (\text{ClO}_2 \text{ asymmetric stretch}), \\
S_8 &= \Delta(\beta_1 - \beta_2)/2^{1/2} && (\text{ClO}_2 \text{ twist}), \\
S_9 &= \Delta\theta && (\text{Cl-O}^*\text{-M out-of-plane deformation}).
\end{aligned}$$

The asterisk in the above descriptions indicates the metal-coordinated oxygen.

A modified valence force field was chosen for the present calculations not only because of the availability from the literature of "free anion" force constants under such an assumption (6), but also because of the good success in the transfer of these force constants from one molecule to another. The potential function which was utilized is given as follows:

$$\begin{aligned}
2V &= \sum_{i=1}^2 K_r (\Delta r_i)^2 + K_R (\Delta R)^2 + K_S (\Delta S)^2 + H_\alpha (\Delta\alpha)^2 \\
&+ \sum_{i=1}^2 H_\beta (\Delta\beta_i)^2 + H_\theta (\Delta\theta)^2 + H_\phi (\Delta\phi)^2 + 2 F_{rr} (\Delta r_1)(\Delta r_2) \\
&+ 2 \sum_{i=1}^2 F_{rR} (\Delta r_i)(\Delta R) + 2 F_{\beta\beta} (\Delta\beta_1)(\Delta\beta_2) + 2 \sum_{i=1}^2 F_{\alpha\beta} (\Delta\beta_i)(\Delta\alpha). \quad (1)
\end{aligned}$$

The Calculations

The first step in the present calculations involving the MClO_3 monomers was to reproduce the "free anion" frequencies. This was accomplished by utilizing the "free anion" force constants (6) ($K_r = K_R = 5.715$ mdyne/A, $F_{rr} = F_{rR} = 0.311$ mdyne/A, $H_\alpha = H_\beta = 2.236 \times 10^{-11}$ ergs/radian², $F_{\alpha\beta} = F_{\beta\beta} = 0.659 \times 10^{-11}$ ergs/radian²) and by equating the force

constants for all modes involving motion to zero ($K_S = H_\theta = H_\phi = 0$) in the potential function previously given. The next step then consisted of changing the bond-stretching force constants of the chlorate ion so that the bond interacting with the metal ion was weakened, while the other two were strengthened. This situation is believed to closely represent the simple polarization of the chlorate ion. At the same time the force constants for modes involving the metal ion were given finite values to include the metal binding.

The calculations were carried out first for the LiClO_3 monomer because of the additional data involving the M-O stretching mode. It was felt that the M-O stretching force constant determined from a fit of the observed frequencies for LiClO_3 could be transferred to the NaClO_3 and KClO_3 monomers in order to obtain a reasonable estimate for the frequency of the M-O stretching mode in these systems. The Li-O stretching force constant for the LiClO_3 monomer was presumed to have a value somewhat less than 2.14 mdyne/\AA , the magnitude of the corresponding force constant in Li_2O (47). The bending constant of $0.035 \times 10^{-11} \text{ ergs/radian}^2$ for Li_2O was used for both the Cl-O-M in-plane and out-of-plane bending constants, H_θ and H_ϕ . These force constants were held fixed at the Li_2O value throughout the calculations for the MClO_3 monomer series. It should be mentioned also that the interaction force constants were held fixed at the "free anion" values.

After obtaining a reasonable fit of the observed frequencies by manually adjusting the force constants in the manner corresponding to anion polarization and metal binding, the next step in the calculation consisted of fitting the force constants by a least squares method to obtain the best possible agreement to the observed frequencies. The

question mentioned in the previous chapter concerning the assignment of the 554 and 533-cm⁻¹ bands for the LiClO₃ monomer was resolved by making two distinct frequency fits. The first was performed with the 554-cm⁻¹ band assigned as the M-O stretching mode and the 533-cm⁻¹ band assigned as the ν_{4b} chlorate mode. For the second calculation these assignments were reversed. The behavior observed for the bending constants, H_α and H_β , in the MClO₃ series was determined to be more in line with the second calculation; therefore, the second assignment became the preferred choice. The calculated frequencies along with potential energy distribution corresponding to this second frequency fit for the LiClO₃ monomer appears in Table X. It should be mentioned that the Ar matrix frequencies were used for the frequency fit. For those bands involving matrix site-splitting, the frequency utilized was either the value of the strongest component or the average value of equal intensity components. It can be seen from Table X that a reasonably good fit of the observed frequencies is obtained with the poorest agreement appearing for the ν_{4a} mode. The potential energy distribution, which gives the percentage contribution of each force constant to a particular frequency, shows that in the A' symmetry block considerable mixing of the ν_2 , ν_{M-O} , and ν_{4a} modes occurs, making it very difficult to justify the assignments given for these modes on the basis of the calculations.

The set of force constants determined from the frequency fit for the LiClO₃ monomer appears in Table XI. For this calculation five force constants which included K_r , K_R , K_S , H_α , and H_β , were adjusted to fit seven frequencies. Also given in Table XI are the final sets of force constants for the NaClO₃ and KClO₃ monomers which correspond to the calculated sets of frequencies given in Tables XII and XIII, respectively.

TABLE X

CALCULATED FREQUENCIES AND POTENTIAL ENERGY DISTRIBUTION FOR THE LITHIUM CHLORATE MONOMER

C _{3v}	Mode	Obs. ^a (cm ⁻¹)	Calc. ^b (cm ⁻¹)	Percentage P.E.D. ^c								
	C _s			K _r	F _{rr} , F _{rR}	K _R	K _S	H _α	F _{αβ} , F _{ββ}	H _β	H _θ	H _φ
v _{3a}	v ₁ (A')	966	967.5	82.3	-0.7	9.6	1.0	8.1	-0.4	0.0	0.0	0.0
v ₁	v ₂ (A')	900	905.7	4.9	3.3	61.3	19.3	0.0	1.8	9.3	0.0	0.0
v ₂	v ₃ (A')	630	650.2	2.5	0.2	0.2	21.8	0.9	18.9	55.0	0.5	0.0
v _{M-0}	v ₄ (A')	533	541.0	5.9	1.1	3.3	21.0	76.4	-10.6	3.0	0.1	0.0
v _{4a}	v ₅ (A')	481	447.4	0.2	-0.4	26.3	36.8	27.3	-13.1	22.7	0.2	0.0
v _{Cl-O-M}	v ₆ (A')	---	87.0	0.0	0.0	0.0	0.0	0.0	0.2	0.5	99.2	0.0
v _{3b}	v ₇ (A'')	1020	1018.3	96.3	-5.0	0.0	0.0	0.0	-2.8	11.4	0.0	0.1
v _{4b}	v ₈ (A'')	557	549.2	9.1	-0.5	0.0	0.0	0.0	-29.2	119.2	0.0	1.3
v _{Cl-O-M}	v ₉ (A'')	---	77.1	0.0	0.0	0.0	0.0	0.0	-0.4	1.8	0.0	98.7

^aAr matrix frequencies.^bAverage error = 2.07%.^cIt was assumed that F_{rr} = F_{rR} and F_{αβ} = F_{ββ} so that only one force constant was used for each pair in the calculation.

TABLE XI
FORCE CONSTANTS USED FOR THE ALKALI-METAL CHLORATE MONOMERS

Force Constant	Coordinates ^a Involved	Force Constant Value ^b		
		LiClO ₃	NaClO ₃	KClO ₃
Stretching				
K _r	Cl-O	6.025	6.077	6.043
K _R	Cl-O*	4.240	4.656	4.804
K _S	M-O*	1.135	1.135	1.135
Bending				
H _α	O-Cl-O	2.295	1.985	2.017
H _β	O-Cl-O*	2.696	2.477	2.440
H _θ	Cl-O*-M (in-plane)	0.035	0.035	0.035
H _φ	Cl-O*-M (out-of-plane)	0.035	0.035	0.035
Interaction				
F _{rr}	Cl-O, Cl-O	0.311	0.311	0.311
F _{rR}	Cl-O, Cl-O*	0.311	0.311	0.311
F _{αβ}	O-Cl-O, O-Cl-O*	0.659	0.659	0.659
F _{ββ}	O-Cl-O*, O-Cl-O*	0.659	0.659	0.659

^aThe asterisk indicates the metal-coordinated oxygen.

^bStretching and stretch-stretch interaction force constants are in units of mdyne/Å. Bending and bend-bend interaction force constants are in units of 10⁻¹¹ ergs/radian².

TABLE XII

CALCULATED FREQUENCIES AND POTENTIAL ENERGY DISTRIBUTION FOR THE SODIUM CHLORATE MONOMER

C_{3v}	Mode	Obs. ^a (cm^{-1})	Calc. ^b (cm^{-1})	Percentage P.E.D. ^c								
	C_s			K_r	F_{rr}, F_{rR}	K_R	K_S	H_α	$F_{\alpha\beta}, F_{\beta\beta}$	H_β	H_θ	H_ϕ
ν_{3a}	ν_1 (A')	972	970.6	77.5	-2.2	17.8	1.3	6.3	-1.0	0.2	0.0	0.0
ν_1	ν_2 (A')	914	914.7	11.3	5.0	62.9	10.0	0.0	2.4	8.3	0.0	0.0
ν_2	ν_3 (A')	622	615.1	3.5	0.7	2.9	6.7	4.0	27.0	54.8	0.5	0.0
ν_{4a}	ν_4 (A')	478	478.6	3.4	0.0	1.8	7.1	101.1	-33.6	21.7	0.0	0.0
ν_{M-O}	ν_5 (A')	---	297.5	0.0	0.0	16.8	74.7	4.8	-3.0	6.3	0.3	0.0
ν_{Cl-O-M}	ν_6 (A')	---	63.3	0.0	0.0	0.1	0.1	0.0	0.2	0.5	99.2	0.0
ν_{3b}	ν_7 (A'')	1017	1018.0	97.9	-5.0	0.0	0.0	0.0	-2.6	9.6	0.0	0.1
ν_{4b}	ν_8 (A'')	518	521.2	7.5	-0.4	0.0	0.0	0.0	-33.3	125.0	0.0	1.2
ν_{Cl-O-M}	ν_9 (A'')	---	52.4	0.0	0.0	0.0	0.0	0.0	-0.5	1.7	0.0	98.8

^aAr matrix frequencies.^bAverage error = 0.36%.^cIt was assumed that $F_{rr} = F_{rR}$ and $F_{\alpha\beta} = F_{\beta\beta}$ so that only one force constant was used for each pair in the calculation.

TABLE XIII

CALCULATED FREQUENCIES AND POTENTIAL ENERGY DISTRIBUTION FOR THE POTASSIUM CHLORATE MONOMER

Mode		Obs. ^a (cm ⁻¹)	Calc. ^b (cm ⁻¹)	Percentage P.E.D. ^c								
C _{3v}	C _s			K _r	F _{rr} , F _{rR}	K _R	K _S	H _α	F _{αβ} , F _{ββ}	H _β	H _θ	H _φ
v _{3a}	v ₁ (A')	968	972.1	70.6	-3.2	25.2	1.9	6.3	-1.4	0.5	0.0	0.0
v ₁	v ₂ (A')	922	920.6	17.9	6.1	57.1	8.4	0.1	2.8	7.6	0.0	0.0
v ₂	v ₃ (A')	627	611.3	3.8	0.7	3.0	5.2	5.0	28.2	53.6	0.5	0.0
v _{4a}	v ₄ (A')	479	479.5	3.3	0.0	0.5	5.3	101.6	-35.4	24.7	0.0	0.0
v _{M-0}	v ₅ (A')	---	249.7	0.0	0.1	14.8	79.0	3.1	-1.9	4.5	0.4	0.0
v _{Cl-O-M}	v ₆ (A')	---	56.7	0.0	0.0	0.1	0.2	0.0	0.2	0.5	99.1	0.0
v _{3b}	v ₇ (A'')	1017	1014.5	98.1	-5.0	0.0	0.0	0.0	-2.5	9.4	0.0	0.1
v _{4b}	v ₈ (A'')	508	515.8	7.3	-0.4	0.0	0.0	0.0	-34.0	126.0	0.0	1.1
v _{Cl-O-M}	v ₉ (A'')	---	46.2	0.0	0.0	0.0	0.0	0.0	-0.4	1.6	0.0	98.9

^aAr matrix frequencies.^bAverage error = 0.83%.^cIt was assumed that F_{rr} = F_{rR} and F_{αβ} = F_{ββ} so that only one force constant was used for each pair in the calculation.

The calculational procedure for both the NaClO_3 and KClO_3 monomers was very similar to that previously described with the exception that the M-O stretching force constant was held fixed at the LiClO_3 monomer value. It is interesting to note that the frequencies calculated for the M-O stretching mode for both the NaClO_3 and KClO_3 monomers are below 300 cm^{-1} which may very well explain why they were not observed. Four force constants were fitted to six frequencies for the NaClO_3 and KClO_3 calculations, and the results obtained are quite good as the average errors indicate.

Discussion

Through the normal coordinate calculations, the expected polarization trend for the MClO_3 monomer series was successfully predicted. One can see from Table XIV that ΔK , which represents the difference between K_r and K_R , decreases through the series from Li to K. This trend can be interpreted in terms of a decrease in the cation polarization of the chlorate anion much like was presented earlier in Table II for the MNO_3 monomer series. The magnitudes of ΔK indicate, however, that the polarization of the chlorate ion is not nearly so great as that observed for the nitrate ion in the MNO_3 monomers. The rather surprising feature, as mentioned before, is the apparent insensitivity of the ν_3 splitting to changes in cation as Table XIV also clearly shows. One does see a very slight trend for this splitting in the Xe matrices as indicated by the numbers in parentheses under the $\Delta\nu_3$ column. The calculations show that the primary effect of increasing ΔK is to decrease the ν_1 frequency while having only a very minor effect on the splitting of ν_3 . Apparently there exists a maximum ΔK value above which one sees very little change for the

splitting of ν_3 . The ΔK for the KClO_3 monomer probably lies very near this limiting value.

TABLE XIV
OBSERVED ν_3 SPLITTINGS IN ARGON AND FORCE
CONSTANT VARIATIONS FOR THE ALKALI-
METAL CHLORATE MONOMERS

M^+	$\Delta\nu_3^a$ (cm^{-1})	K_r^o (mdyne/A)	K_R^o (mdyne/A)	ΔK (mdyne/A)
Li	54 (51)	6.025	4.240	1.785
Na	45 (45)	6.077	4.656	1.421
K	49 (42)	6.043	4.804	1.239

^aThe numbers in parentheses represent the corresponding ν_3 splittings observed in the Xe matrices.

Another aspect of the calculations which deserves some mention is the apparent polarization effect observed for the bending force constants, H_α and H_β . It can be seen in Table XI that H_β assumes a value of somewhat greater magnitude than H_α in each case, with the differences showing only a slight variance throughout the series. The behavior for H_α and H_β is somewhat analogous to that observed for the stretching constants, K_r and K_R , but apparently does not possess the physical meaning that is associated with the stretching force constants.

LiNO_3 Monomer

With the additional data observed in the present reinvestigation of

the LiNO_3 monomer, it was felt that a force constant analysis could be carried out for comparative purposes under assumptions similar to those utilized for the MClO_3 monomers. The model chosen was the same as that utilized for the earlier Urey-Bradley force constant calculations on the MNO_3 monomers (8). The nitrate structural parameters were transferred from the "free anion" (41) and assumed, as for the MClO_3 monomers, to remain unchanged by metal coordination. The parameters used for the nitrate ion were $r_1 = r_2 = R = 1.22 \overset{\circ}{\text{A}}$ and $\beta_1 = \beta_2 = \alpha = 120^\circ$. The Li-O bond distance was assumed to be the same as that used for the LiClO_3 monomer.

The model for the LiNO_3 monomer, which appears in Figure 19, has C_{2v} molecular symmetry; therefore, its nine fundamental vibrational modes are classified as $4A_1 + 3B_1 + 2B_2$. Since the A_1 and B_1 planar modes do not couple with the B_2 out-of-plane modes, an analysis of just the planar vibrations was carried out. Symmetry coordinates were constructed for the seven planar internal coordinates and are given as follows:

for A_1 ,

$$S_1 = \Delta(r_1 + r_2)/2^{\frac{1}{2}} \quad (\text{NO}_2 \text{ symmetric stretch}),$$

$$S_2 = \Delta R \quad (\text{N-O* stretch}),$$

$$S_3 = \Delta(2\alpha - \beta_1 - \beta_2)/6^{\frac{1}{2}} \quad (\text{NO}_2 \text{ scissor}),$$

$$S_4 = \Delta S \quad (\text{M-O* stretch}),$$

$$S_5 = \Delta(\alpha + \beta_1 + \beta_2)/3^{\frac{1}{2}} \quad (\text{redundancy}),$$

for B_1 ,

$$S_6 = \Delta(r_1 - r_2)/2^{\frac{1}{2}} \quad (\text{NO}_2 \text{ asymmetric stretch}),$$

$$S_7 = \Delta(\beta_1 - \beta_2)/2^{\frac{1}{2}} \quad (\text{NO}_2 \text{ rock}),$$

$$S_8 = \Delta\theta \quad (\text{M-O*-N deformation}).$$

In order to remain consistent with the previous calculations, a

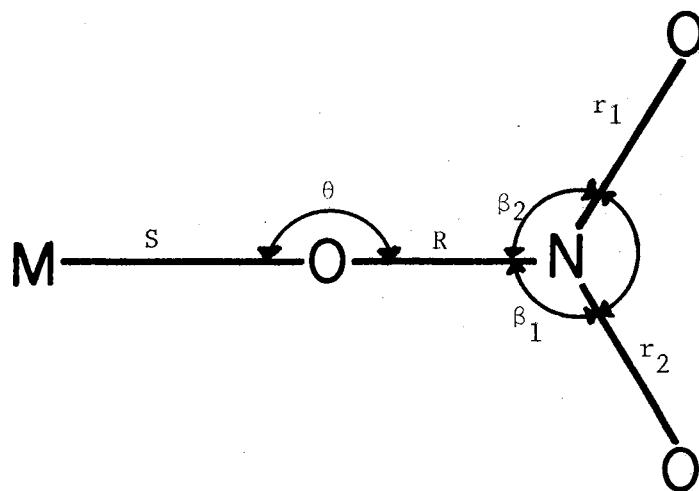


Figure 19. Geometry and Planar Internal Coordinate for the LiNO_3 Monomer

valence force field was again assumed. In attempting to reproduce the "free anion" frequencies, it became necessary to institute several changes in the published set of "free anion" force constants (41) to obtain the desired fit. The potential function for the planar analysis of the LiNO_3 monomer which resulted is given as follows:

$$2V = \sum_{i=1}^2 K_r (\Delta r_i)^2 + K_R (\Delta R)^2 + K_S (\Delta S)^2 + H_\alpha (\Delta \alpha)^2 + \sum_{i=1}^2 H_\beta (\Delta \beta_i)^2 + H_\theta (\Delta \theta)^2 + 2 \sum_{i=1}^2 F_{r\alpha} (\Delta r_i) (\Delta \alpha) + 2 \sum_{i=1}^2 F_{R\beta} (\Delta R) (\Delta \beta_i) + 2F_{r\beta} (\Delta r_1) (\Delta \beta_2) + 2F_{r\beta} (\Delta r_2) (\Delta \beta_1). \quad (2)$$

After satisfactorily reproducing the "free anion" frequencies utilizing the force constants, $K_r = K_R = 6.35 \text{ mdyne/\AA}^0$ (41), $F_{rr} = 2.05 \text{ mdyne/\AA}^0$ (41), $H_\alpha = H_\beta = 2.100 \times 10^{-11} \text{ ergs/radian}^2$ (49), and $F_{r\alpha} = F_{r\beta} = F_{R\beta} = 0.25 \text{ mdyne/radian}$, the calculations which followed for the LiNO_3 monomer were carried out in a manner almost identical to those for the MClO_3 monomer series, including the assumptions made for the force constants involving motion of the metal.

It should be recalled from the LiNO_3 monomer results given in the previous chapter that there was some uncertainty concerning the assignment of the lower-frequency component of the ν_4 nitrate mode. The possibilities for this mode had been narrowed to bands observed at 736 and 692 cm^{-1} ; however, no really definitive judgement in favor of either of these bands could be made. Frequency fits were carried out for both assignments in an attempt to help resolve this question. The calculated frequencies and potential energy distribution for each of the two cases are given in Tables XV and XVI, while the corresponding sets of force constants appear in Table XVII. Although a slightly better frequency fit is obtained for the 736-cm^{-1} assignment, the overall results for

TABLE XV

CALCULATED FREQUENCIES AND POTENTIAL ENERGY DISTRIBUTION FOR THE
PLANAR MODES OF THE LITHIUM NITRATE MONOMER

Mode	Obs. ^a (cm ⁻¹)	Calc. ^b (cm ⁻¹)	Percentage P.E.D. ^c								
			K _r	F _{rr} , F _{rR}	K _R	K _S	H _α	H _β	H _θ	F _{rα} , F _{rβ} , F _{Rβ}	
D _{3h}	C _{2v}										
v _{3a}	v ₁ (A ₁)	1264	1268.0	81.9	-10.2	11.7	0.1	11.8	10.9	0.0	-6.2
v ₁	v ₂ (A ₁)	1011	1024.9	0.6	6.0	60.2	16.5	11.7	10.8	0.0	-5.7
v _{4a}	v ₃ (A ₁)	736	742.6	9.7	-2.0	2.1	51.2	18.8	17.3	0.0	3.0
v _{M-O}	v ₄ (A ₁)	528	492.7	7.9	-17.7	51.3	32.2	10.5	9.6	0.0	6.3
v _{3b}	v ₅ (B ₁)	1524	1532.2	92.9	-22.8	0.0	0.0	0.0	36.6	0.2	-7.0
v _{4b}	v ₆ (B ₁)	765	755.2	40.1	-9.8	0.0	0.0	0.0	63.0	0.6	6.0
v _{N-O-M}	v ₇ (B ₁)	----	79.2	0.0	0.0	0.0	0.0	0.0	0.8	99.2	0.0

^a Ar matrix frequencies

^b Average error = 1.90%.

^c It was assumed that F_{rr} = F_{rR} and F_{rα} = F_{Rβ} and F_{rα} = F_{rβ} = F_{Rβ} so that only one force constant was used for each set in the calculations.

TABLE XVI

CALCULATED FREQUENCIES AND POTENTIAL ENERGY DISTRIBUTION FOR THE
PLANAR MODES OF THE LITHIUM NITRATE MONOMER

D _{3h}	Mode	Obs. ^a (cm ⁻¹)	Calc. ^b (cm ⁻¹)	Percentage P.E.D. ^c							
				K _r	F _{rr} , F _{rR}	K _R	K _S	H _α	H _β	H _θ	F _{rα} , F _{rβ} , F _{Rβ}
v _{3a}	v ₁ (A ₁)	1264	1264.0	85.1	-9.9	12.3	0.1	8.7	9.7	0.0	-6.0
v ₁	v ₂ (A ₁)	1011	1023.7	0.3	4.0	68.2	14.2	9.1	10.2	0.0	-6.0
v _{4a}	v ₃ (A ₁)	692	707.0	7.6	-1.5	1.7	48.5	19.3	21.5	0.0	2.9
v _{M-O}	v ₄ (A ₁)	528	484.2	5.8	-13.1	41.1	37.2	10.8	12.4	0.0	6.2
v _{3b}	v ₅ (B ₁)	1524	1535.4	94.4	-22.8	0.0	0.0	0.0	35.2	0.2	-6.9
v _{4b}	v ₆ (B ₁)	765	752.0	38.1	-9.2	0.0	0.0	0.0	64.5	0.7	5.9
v _{N-O-M}	v ₇ (B ₁)	----	79.2	0.0	0.0	0.0	0.0	0.0	0.8	99.2	0.0

^aAr matrix frequencies.

^bAverage error = 2.53%.

^cIt was assumed that F_{rr} = F_{rR} and F_{rα} = F_{rβ} = F_{Rβ} so that only one force constant was used for each set in the calculation.

TABLE XVII
FORCE CONSTANTS USED FOR THE ALKALI-METAL NITRATE MONOMER

Force Constant	Coordinates ^a Involved	Force Constant Value ^b	
		I ^c	II ^d
	Stretching		
K_r	N-O	8.367	8.474
K_R	N-O*	4.206	4.470
K_S	M-O*	1.539	1.378
	Bending		
H_α	O-N-O	1.143	0.921
H_β	O-N-O*	2.100	2.056
H_θ	N-O*-M (in-plane)	0.035	0.035
	Interaction		
F_{rr}	N-O, N-O	2.050	2.050
F_{rR}	N-O, N-O*	2.050	2.050
$F_{r\alpha}$	N-O, O-N-O	0.250	0.250
$F_{r\beta}$	N-O, O-N-O*	0.250	0.250
$F_{R\beta}$	N-O*, O-N-O*	0.250	0.250

^aThe asterisk indicates the metal-coordinated oxygen.

^bStretching and stretch-stretch interaction force constants are in units of mdyne/Å. Bending force constants are in units of 10^{-11} ergs/radian². Stretch-bend interaction force constants are in units of mdyne/radian.

^cCorresponds to the calculation given in Table XV.

^dCorresponds to the calculation given in Table XVI.

both cases did not differ significantly enough to make any sort of judgement as to which was the correct assignment. The calculations, although rather disappointing in this regard, were still somewhat satisfying in other respects.

Five force constants including K_r , K_R , K_S , H_α , and H_β were fitted to six frequencies for the LiNO_3 calculations with the poorest agreement occurring for the M-O stretching mode in both cases. It appears from the potential energy distributions that the rather large amount of mixing which occurs between the stretching and bending modes in the A_1 symmetry block is responsible for this rather poor fit for $\nu_{\text{M-O}}$.

CHAPTER V

SUMMARY AND CONCLUSIONS

Matrix-Isolated Alkali-Metal Chlorates

The vapors above the molten alkali-metal chlorate salts were characterized by vibrational spectroscopy utilizing the matrix-isolation technique. The spectra clearly indicated that the monomer was a major constituent of the vapors. A detailed study of the monomer vibrational modes was carried out which allowed some very definite conclusions to be made in regard to the structure of this species. It was determined from the splitting of the doubly degenerate ν_3 and ν_4 modes of the chlorate ion that the metal in the monomer was coordinated through the oxygen atoms either in a unidentate or bidentate fashion. Evidence from the limited Raman spectra for the NaClO_3 and KClO_3 monomers tended to favor the unidentate structure. From the available data, the bonding orientation for the metal ion could not be determined.

Normal coordinate calculations were carried out on a model thought to closely represent the MClO_3 monomer. A simple force field, which reproduced the "free anion" frequencies, was chosen. This field was then modified to take into account the metal binding and anion polarization prevalent in the MClO_3 monomers. These calculations were found to yield reasonable estimates of changes in the force field relative to the uncomplexed C_{3v} anion necessary to fit the observed frequencies. In many respects it was gratifying to find that such a simple force field model

as was chosen could be made to agree so well with the experimentally observed data. An analysis of the stretching force constants for the chlorate anion in the $MClO_3$ monomers seemed to indicate that the polarization effect present in these species was not nearly so pronounced as that for the corresponding MNO_3 monomers. The entire study of the $MClO_3$ monomer series led to a better understanding of the perturbing forces which are operative in these systems. This data can be used in gaining further insight into the structures of the molten salts and aqueous solutions as will be discussed in a later section of this chapter.

The vibrational spectra also indicated that certain species other than monomer were present in the vapors above the salts. Dimers, for instance, were readily identified in the matrix spectra for both $NaClO_3$ and $KClO_3$. The tendency to form dimers is apparently greatest for $KClO_3$ as the very large abundance of this species in the most dilute matrix sample indicates. This was a somewhat unexpected result for which no explanation could presently be made. Decomposition was found to be an extremely acute problem in the case of $LiClO_3$. The primary product of this decomposition was identified from both the infrared and Raman spectra as ClO_2 . Traces of O_2 and Cl_2 were also thought to be observed at various times in the Raman spectra. Decomposition was determined to take place only to a very minor extent in the vaporization of both $NaClO_3$ and $KClO_3$.

Alkali-Metal Nitrates

A minor phase of the present investigation consisted of some further studies involving the alkali-metal nitrates. Glass transition temperatures for the glassy films of the alkali-metal nitrates, which were

prepared by vapor deposition in the absence of any matrix gas, were estimated by spectroscopically observing the temperature at which each glass was converted irreversibly to the crystalline solid. These T_g temperatures were compared with those determined from extrapolation of binary solution data and were found to be in some discord with those values. It remains to be determined which set is more nearly correct. Of course, the ideal case for testing the validity of the glass-crystallization T_g values would involve their comparison to the bulk glass values; however, no system has been found yet for which such a comparison can be made.

Thicker films of the matrix-isolated LiNO_3 monomer were examined for vibrational modes which were missed in an earlier study. Both components of the ν_4 bending mode of the nitrate were observed along with M-O stretching mode. This additional vibrational data permitted normal coordinate calculations to be carried out on the LiNO_3 monomer for comparison with MClO_3 monomers.

Volatilization of Polyatomic Salts

The ability to volatilize such polyatomic salts as the alkali-metal chlorates and nitrates is of considerable importance because it adds new dimensions to the study of these species by vibrational spectroscopy. The vapor species can, of course, be isolated in inert matrices to produce an environment in which the anion undergoes maximum distortion or perturbation due to association with a single cation. Knowing the effects that such a limiting case produces on the vibrational spectrum of the anion permits one to make reasonable judgements in regard to amount of anion distortion which might be prevalent in other environments. The

vapors of the salts can also be deposited at low temperatures in the absence of any matrix gas which results in the formation of thin films having a glassy structure. Since the glass structure is believed to be essentially the same as that of the corresponding melt, preparation of the thin glassy films has greatly simplified the infrared spectroscopic study of such structures as well as the measurement of glass transition temperatures.

Another vibrational study which is facilitated by salt volatility is the deliberate placement of metal salt ion pairs (monomers) in other types of matrix environments. Perhaps the most important study of this type involves the use of glassy water as the matrix medium. If the ion pair environment in glassy water is assumed to resemble that for the aqueous solution, then the matrix isolation of the ion pair in glassy water deposits should help to establish the degree of importance of contact ion pairs in such systems.

Correlation with Melt Spectra

As mentioned before the MClO_3 monomer matrix-isolation data can be utilized in gaining some insight into the structure of the melts. Since the vibrational spectrum for the LiClO_3 melt shows considerably more sensitivity than does that of the other MClO_3 melts, the following discussion will be focused primarily on it. It should be recalled from the MClO_3 monomer data that the ν_1 chlorate band position gives perhaps the best handle on determining the extent of distortion or polarization of the chlorate ion under given conditions. Therefore, on the basis of the position of the ν_1 band for the LiClO_3 melt which has been reported at 948 cm^{-1} (5) some 50 cm^{-1} from ν_1 of the LiClO_3 monomer, it can be

concluded that discrete 1:1 ion pairs are apparently not an important consideration in the melt.

A splitting of ca. 65 cm^{-1} has been reported for the ν_3 mode in molten LiClO_3 (5) which is somewhat greater than the 54-cm^{-1} split observed for the monomer. Since the monomer should represent the maximum distortion of the anion, the 65-cm^{-1} split for ν_3 of the melt can obviously not all be due to anion distortion. Devlin, et al. (50), have shown that the 110-cm^{-1} splitting observed for the ν_3 mode in LiNO_3 is due about 65 percent to anion distortion and about 35 percent to a dipole-based dynamical coupling of the two ν_3 components. Such a resonance interaction arises from two closely spaced energy states of the same symmetry which repel each other provided there is a coupling mechanism. The two components of the ν_3 nitrate mode are of the same symmetry in the melt and both have associated large oscillating dipoles; therefore, these two components are forced apart by a resonance interaction through the dipole coupling. Since the ν_3 components for the LiClO_3 melt also meet the above criteria, it is quite likely that the 65-cm^{-1} ν_3 split observed for the melt is due partially to the same type of resonance interaction.

Since it has recently been shown that the cation for the alkali-metal nitrate ion pair is strongly solvated in glassy H_2O and NH_3 matrices (51), it appears risky to draw conclusions for the aqueous solution systems from matrix-isolation data for inert matrices. It does appear likely for the aqueous solution systems such as LiClO_3 , however, that the increased splitting observed for the ν_3 mode with increasing salt concentration can also be explained in terms of the same type of resonance interaction which apparently is prevalent in the melt.

SELECTED BIBLIOGRAPHY

- (1) Angell, C. A., *Ann. Rev. Phys., Chem.*, 22, 453 (1971).
- (2) Irish, D. W., A. R. David, and R. A. Plane, *J. Chem. Phys.*, 50, 2262 (1969).
- (3) Wilmhurst, J. K., *J. Chem. Phys.*, 36, 2415 (1962).
- (4) James, D. W. and W. H. Leong, *Aust. J. Chem.*, 23, 1087 (1970).
- (5) Oliver, B. G. and G. J. Janz, *J. Phys. Chem.*, 75, 2948 (1971).
- (6) Gardiner, D. J., R. B. Girling, and R. E. Hester, *J. Mol. Struct.*, 13, 105 (1972).
- (7) Bates, J. B., A. S. Quist, and G. E. Boyd, *Chem. Phys. Lett.*, 16, 473 (1972).
- (8) Smith, D., D. W. James, and J. P. Devlin, *J. Chem. Phys.*, 54, 4437 (1971).
- (9) Pollard, G., N. Smyrl, and J. P. Devlin, *J. Phys. Chem.*, 76, 1826 (1972).
- (10) Angell, C. A. and D. B. Helphrey, *J. Phys. Chem.*, 75, 2306 (1971).
- (11) Whittle, E., D. A. Dows, and G. C. Pimentel, *J. Chem. Phys.*, 22, 1943 (1954).
- (12) Barnes, A. J. and H. E. Hallam, *Quart. Rev. Chem. Soc.*, 23, 392 (1969).
- (13) Ogden, J. S. and J. J. Turner, *Current Awareness*, 22, 186 (1970).
- (14) Andrews, L., *Ann. Rev. Phys. Chem.*, 22, 109 (1971).
- (15) Hallam, H. E., *Ann. Rep. Chem. Soc.*, 67A, 117 (1970).
- (16) Linevsky, M. J., *J. Chem. Phys.*, 34, 587 (1961).
- (17) Shirk, J. S. and H. H. Claassen, *J. Chem. Phys.*, 54, 3237 (1971).
- (18) Nibler, J. W. and D. A. Coe, *J. Chem. Phys.*, 55, 5153 (1971).
- (19) Ozin, G. A. and A. Vander Voet, *J. Chem. Phys.*, 56, 4768 (1972).

- (20) Levin, I., *Spectrochim. Acta.*, 25A, 157 (1969).
- (21) Ozin, G. A. and A. Vander Voet, *J. Mol. Struct.*, 10, 173 (1971).
- (22) Lesiecki, M., J. W. Nibler, and C. W. DeKnock, *J. Chem. Phys.*, 57, 1352 (1972).
- (23) Boal, D. and G. A. Ozin, *Spectrosc. Lett.*, 4, 43 (1971).
- (24) Claassen, H. H. and J. L. Huston, *J. Chem. Phys.*, 35, 1505 (1971).
- (25) Nibler, J. W., *J. Amer. Chem. Soc.*, 94, 3349 (1972).
- (26) Huber, H. and G. A. Ozin, *J. Mol. Spectrosc.*, 41, 595 (1972).
- (27) Boal, D. H. and G. A. Ozin, *J. Chem. Phys.*, 55, 3598 (1971).
- (28) Andrews, L., Paper I-4, Twenty-seventh Symposium on Molecular Structure and Spectroscopy, Ohio State Univ., June, 1972.
- (29) Li, P. D. and J. P. Devlin, private communication.
- (30) Nakamoto, K., *Infrared Spectra of Inorganic and Coordination Compounds*, Wiley-Interscience, New York, 1970.
- (31) Wong, J. and C. A. Angell, *Appl. Spectrosc. Rev.*, 4, 97 (1970).
- (32) Rawson, H., *Inorganic Glass Forming Systems*, Academic Press, London and New York (1970).
- (33) Kauzmann, W., *Chem. Rev.*, 43, 219 (1948).
- (34) Sugisaki, M., H. Suga, and S. Seki, *Bull. Chem. Soc. Jap.*, 41, 2586 (1968).
- (35) Sugisaki, M., H. Suga, and S. Seki, *Bull. Chem. Soc., Jap.*, 41, 2591 (1968).
- (36) Angell, C. A., private communication.
- (37) *Technical Manual for DisplexTM Model CS-202 Helium Refrigerator*, Air Products and Chemicals, Inc., Allentown, Pennsylvania, September (1971).
- (38) Buchler, A. and J. L. Stauffer, *J. Phys. Chem.*, 70, 4092 (1966).
- (39) Nielsen, A. H. and P. J. Woltz, *J. Chem. Phys.*, 20, 1878 (1952).
- (40) Rochkind, M. M. and G. C. Pimentel, *J. Chem. Phys.*, 42, 1361 (1965).
- (41) Brintzinger, H. and R. E. Hester, *Inorg. Chem.*, 5, 980 (1966).
- (42) Hester, R. E. and W. E. L. Grossman, *Inorg. Chem.*, 5, 1308 (1966).

- (43) McMillan, J. A. and S. C. Los, *Nature (London)*, 206, 806 (1965).
- (44) Angell, C. A. and E. J. Sare, *J. Chem. Phys.*, 52, 1058 (1970).
- (45) Angell, C. A., *J. Phys. Chem.*, 75, 3698 (1971).
- (46) Overend, J., and J. R. Scherer, *J. Chem. Phys.*, 32, 1289, 1296, and 1720 (1960).
- (47) Seshadri, K. S., D. White, and D. E. Mann, *J. Chem. Phys.*, 45, 4697 (1966).
- (48) JANAF Tables of Thermochemical Data, D. R. Stull, ed., Dow Chemical Company, Midland, Michigan (1971).
- (49) Taravel, B. and G. Chauvet, *J. Mol. Struct.*, 13, 283 (1972).
- (50) Devlin, J. P., G. Ritzhaupt, and T. Hudson, *J. Chem. Phys.*, 58, 817 (1973).
- (51) Smyrl, N. and J. P. Devlin, *J. Phys. Chem.*, (in press).

N
VITA

Normal Ray Smyrl

Candidate for the Degree of

Doctor of Philosophy

Thesis: A VIBRATIONAL STUDY OF A SELECTED SERIES OF MATRIX-ISOLATED
ALKALI-METAL CHLORATE AND NITRATE SALTS

Major Field: Chemistry

Biographical:

Personal Data: Born in Littlefield, Texas, March 1, 1946, the son
of Mr. and Mrs. C. W. Smyrl.

Education: Graduate from Canyon High School, Canyon, Texas, in
May, 1964; received Bachelor of Science degree from West Texas
State University, Canyon, Texas, with a major in Chemistry and
minors in Mathematics and Physics, in May, 1969; received the
Master of Science degree from West Texas State University,
with a major in Chemistry, in May, 1971; completed require-
ments for the Doctor of Philosophy degree at Oklahoma State
University in December, 1973.

Professional Experience: Robert A. Welch Foundation Fellow, West
Texas State University, Summer, 1969, through Summer, 1970;
Graduate Teaching Assistant, West Texas State University,
September, 1970 to June, 1971; National Science Foundation
Research Assistant, Oklahoma State University, June, 1971 to
December, 1973; Graduate Teaching Assistant, Oklahoma State
University, September, 1973 to December, 1973.

Membership in Honorary and Professional Societies: Member of Alpha
Chi, Honorary Scholastic Society; member of Phi Lambda Upsilon,
Honorary Chemical Society.